

Beyond maps: Patterns of formation processes at the Middle Pleistocene open-air site of Marathousa 1, Megalopolis Basin, Greece

D. Giusti^{a,*}, V. Tourloukis^a, G. E. Konidaris^a, N. Thompson^a, P. Karkanas^b, E. Panagopoulou^c, K. Harvati^a

^a*Paläoanthropologie, Senckenberg Centre for Human Evolution and Palaeoenvironment, Eberhard Karls Universität Tübingen, Rümelinstr. 23, 72070 Tübingen, Germany*

^b*Malcolm H. Wiener Laboratory for Archaeological Science, American School of Classical Studies at Athens, Greece*

^c*Ephoreia of Palaeoanthropology-Speleology of Greece, Athens, Greece*

Abstract

Recent excavations at the Middle Pleistocene open-air site of Marathousa 1 have unearthed in one of the two investigated areas (Area A) a partial skeleton of a single individual of *Palaeoloxodon antiquus* and other faunal remains in spatial and stratigraphic association with lithic artefacts. In Area B, a much higher number of lithic artefacts was collected, spatially and stratigraphically associated also with faunal remains. The two areas are stratigraphically correlated, the main fossiliferous layers representing an *en masse* depositional process in a lake margin context. Evidence of butchering (cut-marks) has been identified on bones of the elephant skeleton, as well on elephant and other mammal bones from Area B. However, due to the secondary deposition of the main find-bearing units, it is of primary importance to evaluate the degree and reliability of the spatial association of the lithic artefacts with the faunal remains. Indeed, spatial association does not necessarily imply causation, since natural syn- and post-depositional processes may equally produce spatial association. Assessing the degree and extent of post-depositional reworking processes is crucial to fully comprehend the archaeological record, and therefore to reliably interpret past human behaviours. The present study uses a comprehensive set of spatial statistics in order to disentangle the depositional processes behind the distribution of the archaeological and palaeontological record at Marathousa 1. Preliminary results of our analyses suggest minor reworking and substantial spatial association of the lithic and faunal assemblages, supporting the current interpretation of Marathousa 1 as a butchering site.

Keywords: Spatial analysis, Site formation processes, Vertical distribution, Fabric analysis, Point pattern analysis, Middle Pleistocene

*Corresponding author

Email address: domenico.giusti@uni-tuebingen.de (D. Giusti)

1 **1. Introduction**

2 Archaeological site formation processes, intensively studied since the early 1970s
3 ([Isaac, 1967](#); [Schiffer, 1972, 1983, 1987](#); [Shackley, 1978](#); [Wood and Johnson, 1978](#);
4 [Binford, 1981](#); [Schick, 1984, 1986, 1987](#); [Petraglia and Nash, 1987](#); [Petraglia and](#)
5 [Potts, 1994](#), among others), “still insufficiently taken in consideration” ([Texier, 2000](#),
6 p.379) at the beginning of the 21st century, are nowadays fully acknowledged in the ar-
7 chaeological practice ([Villa, 2004](#); [Bailey, 2007](#); [Brantingham et al., 2007](#); [Malinsky-](#)
8 [Buller et al., 2011](#); [Vaquero et al., 2012](#); [Bargalló et al., 2016](#), among others). Drawing
9 inferences about past human behaviours from scatters of archaeological remains must
10 account for syn- and post-depositional contextual processes.

11 Several methods are currently applied in order to qualify and quantify the type and
12 degree of reworking of archaeological assemblages. Within the framework of a geoar-
13 chaeological and taphonomic approach, spatial statistics offer meaningful contributions
14 in unravelling site formation and modification processes from spatial patterns. How-
15 ever, while the spatio-temporal dimension is an ineluctable inherent property of any
16 biotic and abiotic process, spatial statistics are still insufficiently applied.

17 Distribution maps are cornerstones of the archaeological documentation process
18 and are primary analytic tools. However, their visual interpretation is prone to subjec-
19 tivity and is not reproducible ([Bevan et al., 2013](#)). Since the early 1970's (see [Hodder](#)
20 and [Orton \(1976\)](#); [Orton \(1982\)](#) and references therein), the traditional, intuitive, ‘eye-
21 balling’ method of spotting spatial patterns has been abandoned in favour of more ob-
22 jective approaches, extensively borrowed from other fields. Nevertheless, quantitative
23 methods, while still percolating in the archaeological sciences from neighbouring dis-
24 ciplines, are not extensively used. Moreover, only a relatively small number of studies
25 have explicitly applied spatial point pattern analysis or geostatistics to the study of site
26 formation and modification processes ([Lenoble et al. \(2008\)](#); [Domínguez-Rodrigo et al.](#)
27 ([2014b,a, 2017](#)); [Carrer \(2015\)](#); [Giusti and Arzarello \(2016\)](#); [Organista et al. \(2017\)](#) -
28 but see [Hivernel and Hodder \(1984\)](#) for an earlier work on the subject).

29 The goal of a taphonomic approach to spatial analysis is to move beyond distri-
30 bution maps by applying a comprehensive set of multiscale and multivariate spatial
31 statistics in order to reliably construct inferences from spatial patterns. An exhaustive
32 spatial analytic approach to archaeological inference, combined with a taphonomic
33 perspective, is essential for evaluating the depositional processes and integrity of the
34 archaeological assemblage, and consequently for a reliable interpretation of past hu-
35 man behaviours.

36 The present study uses a comprehensive set of spatial statistics in order to disentan-
37 gle the depositional processes behind the spatial distribution of the archaeological and
38 palaeontological record recovered during excavation at the Middle Pleistocene open-air
39 site of Marathousa 1, Megalopolis, Greece ([Panagopoulou et al., 2015](#); [Harvati et al.](#),
40 [2016](#)).

41 **1.1. Marathousa 1**

42 The site (Fig. 1), discovered in 2013 at the edge of an active lignite quarry, is
43 located between two lignite seams in the Pleistocene deposits of the Megalopolis basin,
44 Marathousa Member of the Choremi Formation ([van Vugt et al., 2000](#)). The regular

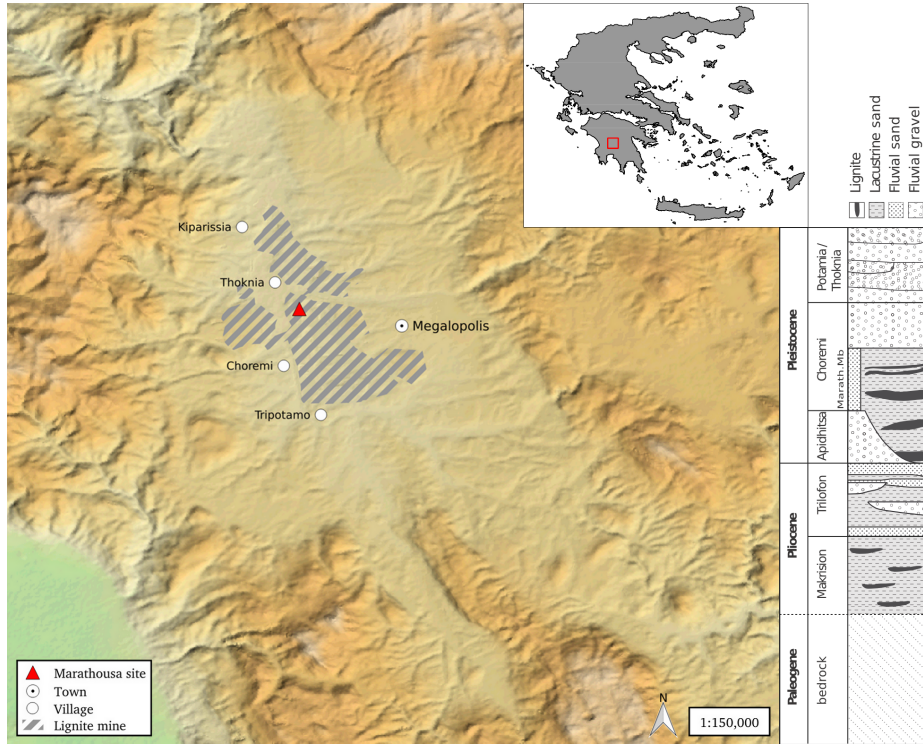


Figure 1: Geographical location of the Marathousa 1 site in the Megalopolis basin and stratigraphic column of the basin, modified after [van Vugt et al. \(2000\)](#).

45 alternation of lacustrine clay, silt and sand beds with lignite seams has been interpreted
 46 having cyclic glacial (or stadial) and interglacial (or interstadial) origin ([Nickel et al., 1996](#)). The half-graben configuration of the basin, with major subsidence along the
 47 NW-SE trending normal faults along the eastern margin, resulted in the gentle dip of
 48 the lake bottom at the opposite, western, margin of the lake, enabling the formation of
 49 swamps and the accumulation of organic material for prolonged periods of time ([van
 50 Vugt et al., 2000](#)).

51 Two excavation areas have been investigated since 2013 (Fig. 2): Area A, where
 52 several skeletal elements of a single individual of *Palaeoloxodon antiquus* have been
 53 unearthed, together with a number of lithic artefacts; and Area B, located 60 m to
 54 the South along the exposed section, where the lithic assemblage is richer and occurs
 55 in association with a faunal assemblage composed of isolated elephant bones, cervids
 56 and carnivores among others ([Konidaris et al., this issue](#); [Tourloukis et al., this issue](#)).
 57 Evidence of butchering (cut-marks) have been identified on two of the elephant bones
 58 from Area A, as well on elephant and other mammal bones from Area B ([Konidaris
 59 et al., this issue](#)).

60 The sedimentary sequence of the site (Fig. 3) includes lacustrine and fluvio-lacustrine
 61 clastic deposits sandwiched between two lignite seams (UA7-UB10 and UA1-UB1)

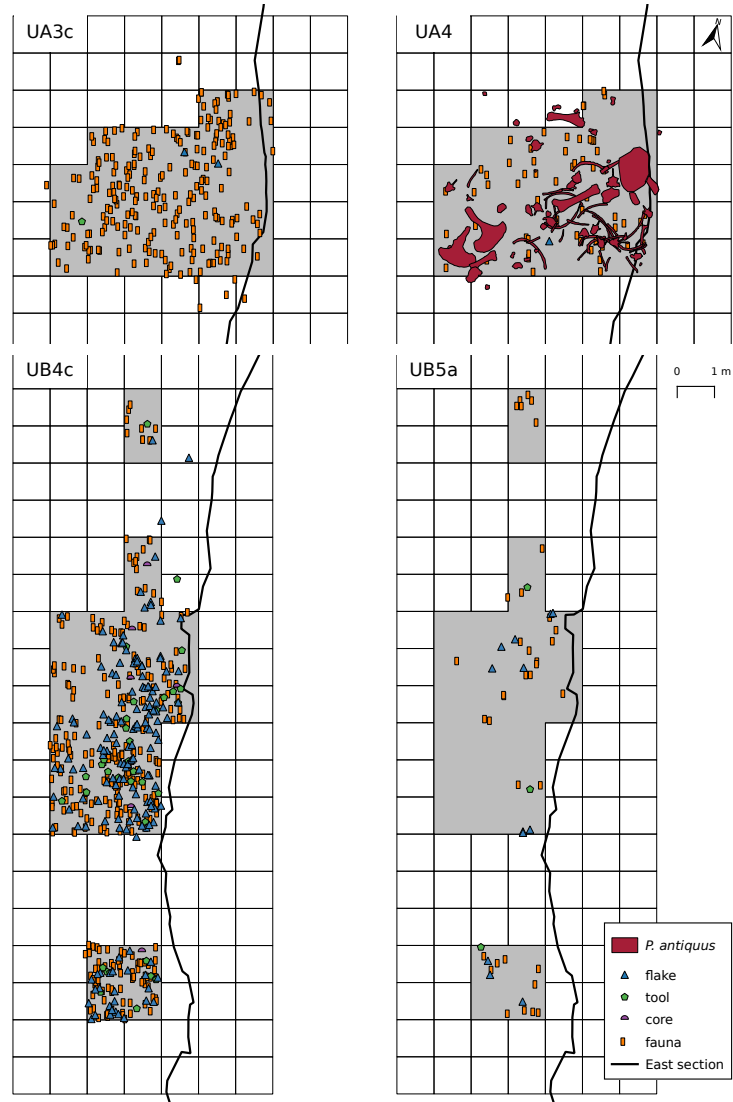


Figure 2: Distribution maps of the plotted remains from areas A (units UA3c and UA4) and B (units UB4c and UB5a). Grey zones mark the 2013-2015 excavation areas. The plotted remains of the *P. antiquus* skeleton were collected until 2016. Area B is located 60 m to the South, along the exposed East section of the lignite quarry.

(Karkanas et al., this issue). A major hiatus (contacts between UA3 and UA4, and between UB5 and UB6), attributed to exposure and erosion of a lake shore mudflat, divides the sequence in two parts. The lower part is characterised by relatively high rate sub-aqueous sedimentation of bedded sands and silts, containing low organic and carbonate content. The upper one is characterised by a series of erosional bounded depositional units, attributed to sub-aerial originated organic- and carbonate-rich mud flows and hyperconcentrated flows deposited at the margin of a swamp (Karkanas et al., this issue).

The erosional contacts UA3c/4 and UB4c/5a separate the two main find-bearing units in both areas. In Area A, the elephant remains lie at the contact of UA3c/4 and are covered by UA3c (Fig. 4a); while in Area B, most of the remains were collected from unit UB4c (Fig. 4b). Units UA3c and UB4c (organic- and intraclast-rich silty sands) resemble dilute mud flows, showing a chaotic structure of rip-up clasts from the underlying unit, small-to-large wood fragments and rare rock clasts. In Area B, a relatively low number of remains was also found in massive organic-rich silty sands (UB5a), which locally overlay channelised sands (UB5b/c), probably not preserved in Area A (Karkanas et al., this issue).

The flow event described above (units UA3c and UB4c), and specifically the erosional contacts between the fossiliferous horizons in the two areas (UA3c/4 and UB4c/5a), provide the essential background for the analysis and interpretation of the spatial distributions at Marathousa 1.

The secondary depositional nature of the main find horizons raises the question of how reliable is the spatial association between the lithic artefacts and the partial skeleton of a single *Palaeoloxodon antiquus* individual and other faunal remains. Since spatial association does not necessarily imply causation, and consequently synchrony, the answer has important consequences for the interpretation of the site in the broader context of the Middle Pleistocene human-proboscidean interactions. We aim to tackle this question and disentangle the formation processes acting at Marathousa 1 on the basis of spatial patterns through a three-prong spatial analytic approach:

1. by analysing, in a frame of references, the orientation patterns of remains from relevant stratigraphic units;
2. by quantifying and comparing their relative vertical distributions;
3. by identifying spatial trends in either the assemblage intensities and the associations between classes of remains.

Two contrasting models of deposition are tested: the autochthonous hypothesis (*sensu* Fernández-López, 1991; Domínguez-Rodrigo et al., 2012) states that the flow event, represented by units UA3c and UB4c, eroded and scoured the exposed surface (where the elephant was lying), thereby entraining clastic material (including artefacts) and re-depositing (*sensu* Fernández-López, 1991) this material at a close distance. This model implies the loss of any original, pristine spatial relations between remains, but minor transport from the primary depositional *loci*. On the other hand, the allochthonous hypothesis (*sensu* Fernández-López, 1991; Domínguez-Rodrigo et al., 2012) implies significant transport from the original *loci* of deposition and re-elaboration (*sensu* Fernández-López, 1991). According to this model, the spurious spatial associ-

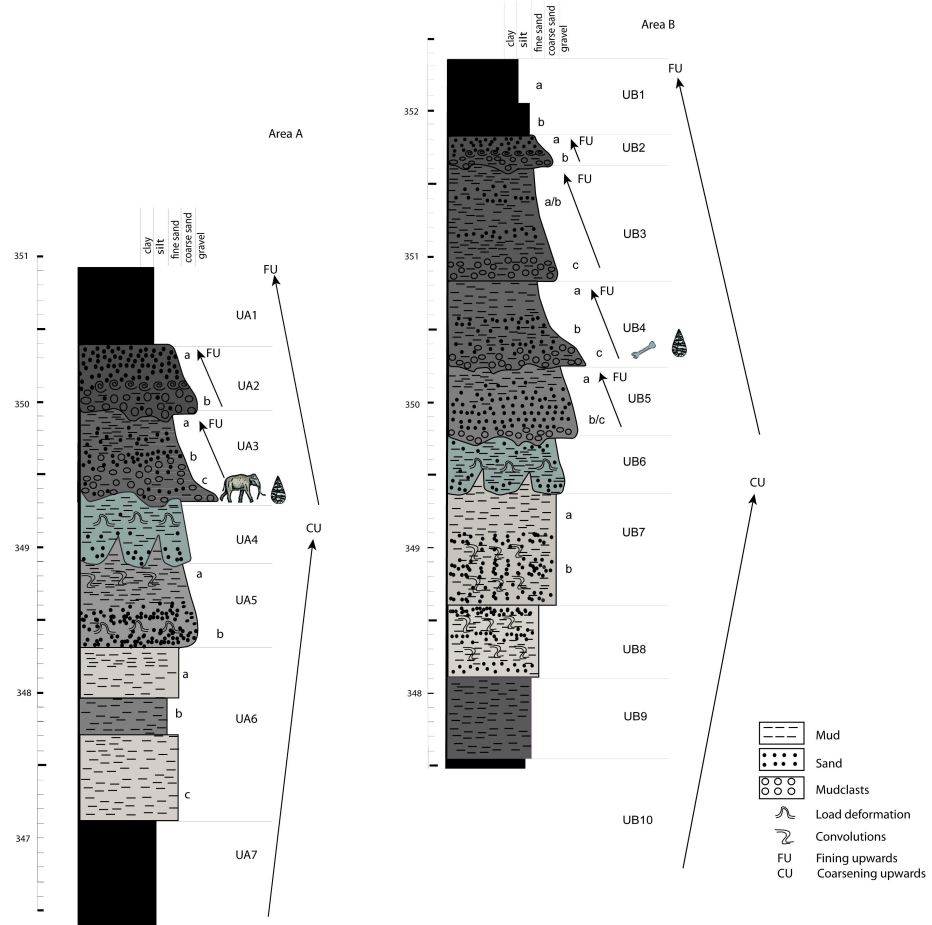


Figure 3: Stratigraphic setting of the Marathousa 1 site, modified after Karkanas et al. ([this issue](#)). Absolute elevations in m a.s.l.

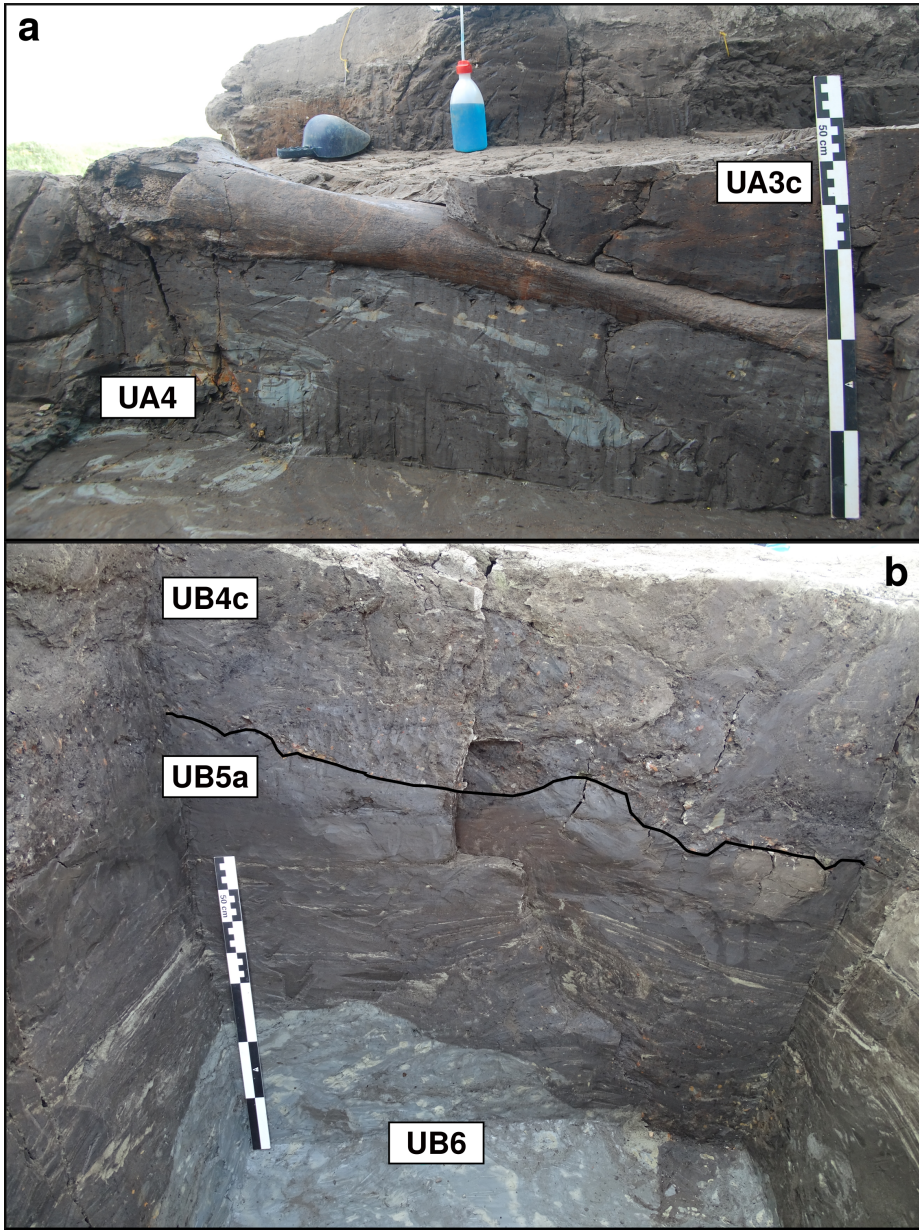


Figure 4: Photograph (2017) of the left femur of the *P. antiquus* skeleton, lying at the UA3c/4 contact and covered by unit UA3c (a). West profile (2014) of the excavation Area B (square 932/603), exposing the UB4c/5a (black solid line) and the UB5c/6 erosional contacts (b).

107 ation between the lithic artefacts and faunal remains does not support any behavioural
108 interpretation.

109 **2. Material and methods**

110 Since 2013, systematic investigation of the Marathousa 1 site has been carried out
111 by a joint team from the Ephoreia of Palaeoanthropology-Speleology (Greek Ministry
112 of Culture) and the University of Tübingen. A grid system of 1 square meter units
113 was set up, oriented -14 degrees off the magnetic North, and including the two areas
114 of investigation. The excavation of the deposit proceeded in 50x50 cm sub-squares
115 in Area B and 1x1 m squares in Area A, and spits of 5 to 10 cm thickness, respec-
116 tively. Systematic water-screening of sediments was carried out on-site using 1 mm
117 sieves in order to guarantee recovery of the small-size fraction (e.g., micro-artefacts,
118 small mammal remains, fish, molluscs and small fragments of organic and inorganic
119 material). The three-dimensional coordinates of finds (i.e., all the lithic artefacts, teeth
120 and diagnostic bones; bones and organic material with a-axis ≥ 20 mm), collected
121 spits of sediment, samples and geological features (e.g., erosional contacts and mud
122 cracks) were recorded with a Total Station. Dense clouds of surface points of the ele-
123 phant skeletal elements were acquired using both a Total Station and a close-range
124 photogrammetric technique.

125 The dimensions (length, width and thickness) of registered finds were measured
126 on-site with millimetre rules. Orientation (plunge and bearing) of elongated particles
127 (i.e., faunal remains, large wood fragments and lithic artefacts) was recorded since
128 2013 using a clock-like system (the bearing was measured, relatively to the grid North,
129 in twelve clockwise intervals of 30°; the plunge with a 22.5° accuracy). In 2015, the
130 use of a compass and inclinometer with an accuracy of 1° was introduced in Area B to
131 gradually replace the former method.

132 The widespread use of a compass and inclinometer to record orientation data (Voorhies,
133 1969; Fiorillo, 1991; Bertran and Texier, 1995; Bertran et al., 1997; Lenoble and
134 Bertran, 2004; Eberth et al., 2007; Eren et al., 2010; Benito-Calvo et al., 2011; Domínguez-
135 Rodrigo et al., 2012; Domínguez-Rodrigo and García-Pérez, 2013; Domínguez-Rodrigo
136 et al., 2014c; Cobo-Sánchez et al., 2014; Organista et al., 2017, among others) was
137 favoured over the alternative use of a total station (Kluskens, 1990; Dibble et al., 1997;
138 McPherron, 2005; Enloe, 2006; Bernatchez, 2010, among others), mostly due to the
139 time-restricted conditions of the rescue excavation conducted at Marathousa 1.

140 Measurements of the bearing (azimuth) and plunge (dip) of elongated finds were
141 taken along the symmetrical longitudinal a-axis (SLA) of bones (Domínguez-Rodrigo
142 and García-Pérez, 2013), lithic artefacts (Bertran and Texier, 1995) and wood frag-
143 ments (Macdonald and Jefferson, 1985), using the lowest endpoint of the a-axis as an
144 indicator of the vector direction.

145 Other major axes have been alternatively used with the recent application of GIS
146 techniques to retrieve orientation data from secondary source (i.e., excavation pho-
147 tographs, drawings or maps) (Boschian and Saccà, 2010; Benito-Calvo and de la Torre,
148 2011; de la Torre and Benito-Calvo, 2013; Walter and Trauth, 2013; García-Moreno
149 et al., 2016; Sánchez-Romero et al., 2016). However, the experimental works of Domínguez-
150 Rodrigo and García-Pérez (2013) and Domínguez-Rodrigo et al. (2014c) showed that

151 the SLA, defined as the major axis which symmetrically divide the bone, is more accurate
152 in determining the preferential orientation of anisotropic assemblages. This a-axis
153 is widely used in taphonomic studies (Toots, 1965; Voorhies, 1969; Eberth et al., 2007;
154 Domínguez-Rodrigo et al., 2012, 2014a; Aramendi et al., 2017, among others) and, as
155 the artefact major axis (Krumbein, 1941), in studies which employ a sedimentological
156 approach to archaeological fabric (Bertran and Texier, 1995; Bertran et al., 1997;
157 Lenoble and Bertran, 2004; Benito-Calvo et al., 2009, among others).

158 The present study focuses on the excavated stratigraphic units in which most of the
159 archaeological and palaeontological remains were recovered in both excavation areas,
160 namely in UA3c and UA4 in Area A, and UB4c and UB5a in Area B. From the total,
161 subset samples of material were used for each specific spatial analysis. For the fabric
162 analysis we included material collected until 2016. For the vertical distribution and
163 point pattern analyses, the region of investigation was limited to the squares excavated
164 from 2013 until 2015, 25 and 29 square meters respectively in each area.

165 The analyses were performed in R statistical software (R Core Team, 2017). In
166 order to make this research reproducible (Marwick, 2017; Marwick et al., 2017), a
167 repository containing a compendium of data, source code and text is open licensed and
168 available at the DOI: [10.5281/zenodo.822273](https://doi.org/10.5281/zenodo.822273)

169 2.1. Fabric analysis

170 The taphonomic study of the orientation pattern of elongated sedimentary particles,
171 including bones and artefacts, first addressed by Voorhies (1969); Isaac (1967); Bar-
172 Yosef and Tchernov (1972); Schick (1986), more recently led to a noteworthy develop-
173 ment of methods and propagation of applications in Palaeolithic site formation studies
174 (Bertran and Texier, 1995; Bertran et al., 1997; Lenoble and Bertran, 2004; Lenoble
175 et al., 2008; McPherron, 2005; Benito-Calvo et al., 2009, 2011; Benito-Calvo and de la
176 Torre, 2011; Bernatchez, 2010; Boschian and Saccà, 2010; Domínguez-Rodrigo et al.,
177 2012; Domínguez-Rodrigo and García-Pérez, 2013; Domínguez-Rodrigo et al., 2014c;
178 de la Torre and Benito-Calvo, 2013; Walter and Trauth, 2013; García-Moreno et al.,
179 2016; Sánchez-Romero et al., 2016, among others).

180 Fabric analysis can provide valuable insight into site formation and taphonomic
181 processes, allowing discrimination between different orientation patterns (isotropic,
182 linear or planar) associated with a range of sedimentary processes. Whereas water-flow
183 deposits are generally characterised by relatively good sorting and preferred orientation
184 of clasts parallel, or normal to the flow direction (linear fabric) (Petruglia and Potts,
185 1994); debris-flow deposits mostly exhibit massive, poorly bedded mixtures of un-
186 sorted sediments and random orientation of clasts (isotropic fabric), except at the flow
187 margins where linear fabric may occur (Pierson, 2005). On the other hand, undisturbed
188 archaeological sites, as well as experimental sites, have been observed to have planar
189 fabric (Bertran et al., 1997; Lenoble and Bertran, 2004). Nevertheless, grey zones exist
190 between depositional processes, so that an unequivocal discrimination based only on
191 fabric observations is often not possible, and other taphonomic criteria must also be
192 considered (Lenoble and Bertran, 2004). As an example, while overland flows (runoff)
193 have been observed to show some degree of planar fabric (Lenoble and Bertran, 2004),
194 anisotropy without significant transport can be caused in a lacustrine floodplain by low-

195 energy processes such as lake transgression and regression, as well as water-sheet flows
196 formed during rainy seasons (Cobo-Sánchez et al., 2014).

197 At the margin of a lacustrine environment, relatively close to the surrounding relief,
198 a combination of high- and low-energy processes can be expected. According to
199 the sedimentological and micromorphological study of the Marathousa 1 site, the main
200 find-bearing horizon is associated with hyperconcentrated flows (Karkanas et al., this
201 issue). Hyperconcentrated flows are intermediate states, defined by sediment concen-
202 tration, in the continuum between sub-aerial water flows and debris flows. Benvenuti
203 and Martini (2002) reported that, when a turbulent hyperconcentrated flow expands
204 over a surface - as in the case of Marathousa 1 - a two-phase flow may develop, with a
205 more concentrated, coarser grained bottom flow-layer (traction carpet) moving slower
206 than the upper turbulent flow-layer carrying wash-load and suspended load. Resultant
207 deposit may exhibit diagnostic inverse grading, or a continuously aggrading bed. Paral-
208 lel or normal orientation of the clasts to the flow direction can be observed (Benvenuti
209 and Martini, 2002). A simulation model also showed that linear fabric can develop in
210 mud flows. However, after deposition, settling of the clasts may affect the fabric to
211 some extent, depending on the viscosity of the mud flow (Lindsay, 1968).

212 As part of our three-prong spatial analytic approach, we conducted comparative
213 fabric analysis with the aim to investigate the dynamics of the depositional processes
214 at Marathousa 1.

215 Since fabric strength has been found to be positively correlated with the shape and
216 size of the clast, for the fabric analysis we subset samples of remains with length \geq 2 cm
217 and elongation index (the ratio length/width) $I_e \geq 1.6$ (Lenoble and Bertran, 2004). The
218 samples are listed in Table 1 and include mostly wood fragments and faunal remains
219 from the four stratigraphic units under investigation. Bones have been found to readily
220 react to water flow and show very early anisotropic patterns (Domínguez-Rodrigo et al.,
221 2014c). Flume experiments showed that wood fragments as well tend to align parallel
222 to the current direction (Macdonald and Jefferson, 1985). No distinction of skeletal
223 elements was made, both due to the high fragmentation rate of faunal remains in Area
224 B, and because recent experiments showed a similar orientation pattern for different
225 bone shapes (Domínguez-Rodrigo et al., 2012; Domínguez-Rodrigo and García-Pérez,
226 2013).

227 The sample of bones belonging to the individual of *P. antiquus* from Area A was
228 analysed separately and included the humerus, ulna, femur and tibia; the atlas, axis and
229 other 16 complete vertebrae or vertebral fragments; 29 complete ribs or rib fragments;
230 2 calcanea; 4 metatarsals/metacarpals; the pyramidal; the trapezoid and the pelvis. The
231 sample from UB5a was too small (only 7 observations) and was therefore excluded. In
232 order to asses the reliability of the orientation data recorded using the clock method,
233 we separately analysed two sub-samples from unit UB4c, selected from a set of finds
234 recorded using both methods. All the sampled observations are representative of the
235 whole study area.

236 Rose diagrams and uniformity tests, such as Rayleigh, Kuiper, Watson and Rao
237 tests (Jammalamadaka et al., 2001), were used to visualise and evaluate circular isotropy
238 in the sample distribution. The Rayleigh test is used to assess the significance of the
239 sample mean resultant length (\bar{R}), assuming that the distribution is unimodal and not
240 bi- or plurimodal. The \bar{R} ranges from 0 to 1: values close to 1 indicate that the data are

Table 1: List of sampled observations for the fabric analysis.

| Sample | <i>n</i> | Type | | |
|--------------------|----------|-------|------|--------|
| | | Fauna | Wood | Lithic |
| UA3c | 49 | 23 | 25 | 1 |
| UA4 | 38 | 8 | 30 | - |
| <i>P. antiquus</i> | 63 | | | |
| UB4c | 38 | 30 | 1 | 7 |

241 closely clustered around the mean direction; when the data are evenly spread \bar{R} has a
 242 value close to 0. A *p* – *value* lower than 0.05 rejects the hypothesis of uniformity with
 243 a 95% confidence interval. Kuiper, Watson and Rao are omnibus tests used to detect
 244 multimodal departures from circular uniformity. The test results are evaluated against
 245 critical values: a result higher than the critical value rejects with confidence the null
 246 hypothesis.

247 Randomness testing of three-dimensional data was conducted with the Woodcock
 248 S_1/S_3 test ([Woodcock and Naylor, 1983](#)). Considering both the plunge and bearing
 249 of the oriented items, this method, based on three ordered eigenvalues (S_1, S_2, S_3), is
 250 able to discriminate the shape and strength of the distributions. The shape parameter
 251 $K = \frac{\ln(S_1/S_2)}{\ln(S_2/S_3)}$ ranges from zero (uni-axial girdles) to infinite (uni-axial clusters). The
 252 parameter $C = \ln(S_1/S_3)$ expresses the strength of the preferential orientation, and
 253 its significance is evaluated against critical values from simulated random samples of
 254 different sizes. A perfect random uniform distribution would have $C = 0$ and $K = 1$.

255 The Benn diagram ([Benn, 1994](#)) adds to the Woodcock test an isotropy ($IS =$
 256 S_3/S_1) and an elongation ($ES = 1 - (S_2/S_1)$) index. Like the former method, it is
 257 able to differentiate between linear (cluster), planar (girdle) or isotropic distributions.
 258 There are no published raw data from actualistic studies on hyperconcentrated flows or
 259 other depositional processes affecting the orientation of bones and artefacts deposited
 260 on lacustrine floodplains (but see [Morton \(2004\)](#) and [Cobo-Sánchez et al. \(2014\)](#) as
 261 pioneer studies on this subject). However, we included in the Benn diagram relevant
 262 references to published results from observation of fabrics in modern subaereal slope
 263 deposits, i.e., debris flow and runoff ([Bertran et al., 1997](#); [Lenoble and Bertran, 2004](#)).

264 2.2. Vertical distribution

265 The vertical distribution of materials has been long investigated with the aim of
 266 identifying cultural levels, by visually interpreting cross-sectional plots. However,
 267 recent advances in GIS techniques allow to inspect at higher resolution the three-
 268 dimensional distributions of archaeological remains ([McPherron et al., 2005](#); [Anderson](#)
 269 and [Burke, 2008](#), among others).

270 In analysing the vertical dispersion of material at Marathousa 1, we provisionally
 271 assume that a general concentration of unsorted lithic artefacts and faunal remains in
 272 the proximity of the erosional surfaces would support an autochthonous origin of the
 273 assemblages; whereas a homogeneous vertical distribution of remains from the UA3c
 274 and UB4c units would suggest an allochthonous origin, significant transport and subse-
 275 quent re-deposition of the material. Indeed, massive process such as hyperconcentrated

Table 2: List of sampled observations for the vertical distribution and point pattern analyses.

| Sample | <i>n</i> | Lithic class | | | | | Faunal class | | | |
|--------|----------|--------------|-------|------------|------|------|--------------|------|-------|------------|
| | | Debris/chip | Flake | Bone flake | Tool | Core | Indet. | Bone | Tooth | Microfauna |
| UA3c | 279 | 46 | 2 | - | 1 | - | 1 | 171 | 14 | 44 |
| UA4 | 61 | 3 | 1 | - | - | - | - | 45 | 4 | 8 |
| UB4c | 1243 | 753 | 154 | 1 | 34 | 6 | 2 | 246 | 28 | 19 |
| UB5a | 101 | 50 | 12 | - | 3 | - | - | 30 | 3 | 3 |

flows, have high erosional power and rather chaotic structure, which may result in inverse or normal grading ([Benvenuti and Martini, 2002](#)).

In order to estimate the degree of vertical dispersion while controlling for the size of the archaeological material, dimensional classes were set up following typological criteria. Lithic artefacts were classified as debris/chips when smaller than a cutoff length of 15 mm ([Tourloukis et al., this issue](#)). Other classes include flakes, tools and cores; the latter being the bigger and heavier debitage product. Table 2 summarises the sample size for each class. Lithic debris/chips constitute the larger part of the assemblage from UB4c (60%) and UB5a (49%); whereas in Area A they represent only a moderate percentage in the upper UA3c unit (16%). The very rare presence of lithic artefacts in the underlying unit UA4 is nevertheless significant. In this unit, the faunal remains are also found in much lower numbers, their number reduced to one fourth of those found in UA3c. For the point pattern analysis (see below), we used the same subset of material for both excavation areas.

For Area B, the material recovered from the water-screening was randomly provenanced according to the 5 cm depth of the excavated spit and the coordinates of the 50x50 cm quadrant of the excavation square. Following the same excavation protocol, the same procedure was applied for the water-screened material of Area A, which was randomly provenanced according to 3D-coordinates of the 1x1 m excavation square and 10 cm spit.

Ordinary Kriging interpolation of the recorded points of contact between the UA3c/UA4 and the UB4c/UB5a stratigraphic units were used to reconstruct the UA3c/4 and UB4c/5a erosional surfaces (Fig. 5a,b). In geostatistics, Kriging is a method of interpolation which, from a modelled function of spatial autocorrelation between known points (e.g., recorded elevations), calculates values of unknown points (e.g., predicted elevations). Thus, in order to address our specific objective, i.e., to quantify and analyse the vertical distribution of the archaeological and palaeontological material, we measured the minimum orthogonal distance (*d*) of each specimen to the interpolated erosional surface (Fig. 5c). For the units above and below this surface (i.e., UB4c and UB5a), the relative distribution of lithic classes and faunal remains was informally tested by means of kernel density estimations.

In Area A, the UA3c/4 erosional contact is locally sharp, but, in contrast to Area B, parts of the eroded unit UA4 are mixed with pockets of the UA3c organic-rich silty sands and intraclast-rich mud flows ([Karkanas et al., this issue](#)). However, from sparse known points of the erosional contact, the UA3c/4 surface was interpolated and the vertical dispersion of remains estimated as well. The elephant remains were excluded from this analysis, since they clearly lie horizontally at the UA3c/4 contact (Fig. 4a and

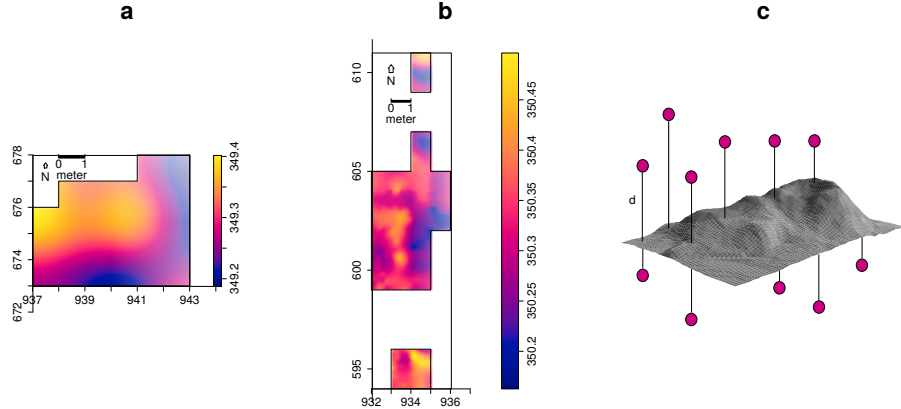


Figure 5: Ordinary Kriging interpolation of the UA3c/4 (a) and UB4c/5a (b) erosional surface; the colour scale denotes absolute elevation in m a.s.l. (c) Illustration of the method used to quantify the vertical dispersion of remains (d) with respect to the UA3c/4 (a) and UB4c/5a (b) surface.

313 SI).

314 Finally, a Student's two sample t-test allowed us to compare the empirical distributions
315 of different groups of remains for each stratigraphic unit.

316 *2.3. Point pattern analysis*

317 A spatial point pattern is defined as the outcome of a random spatial point process
318 (repetitions of it would always create a different pattern). The observed patterns of the
319 archaeological and palaeontological remains were treated as manifestations of spatial
320 point processes, i.e., site formation processes. Point pattern analysis investigates the
321 spatial arrangement of points with the aim of identifying spatial trends. In order to
322 integrate the previous studies of the fabric and vertical distributions, we directed our
323 point pattern analysis equally to the intensity of the patterns (the rate of occurrence of
324 the recorded finds) and to the spatial interaction between different types of finds.

325 As the average number of random points per unit area, intensity informs about
326 homogeneity or inhomogeneity in the distribution of events (e.g., clasts) generated by
327 a point process (e.g., mud flow), i.e., whether the rate of occurrence is uniform or
328 spatially varying across the study area. Intensity, usually non-parametrically evaluated
329 by means of kernel density estimation ([Diggle, 1985](#)), was assessed for the distribution
330 of material from the UB4c, UB5a and UA3c units. Cross-validation bandwidth, which
331 assumes a Cox process, and edge correction were applied using the methods described
332 in [Diggle \(1985\)](#).

333 In the presence of a covariate, it is recommended to further investigate the dependence
334 of intensity on that explanatory variable ([Baddeley et al., 2012](#)). In order to evaluate whether variation in the density of materials was correlated to the topography
335 of the erosional surface, we computed a local likelihood smoothing estimate of the in-
336 tensity of remains from UB4c as a function of the UB4c/5a surface elevation model.
337 Formal tests enabled us to assess the evidence of that dependence and to quantify the
338

strength of the covariate. The Kolmogorov-Smirnov test of CSR (Complete Spatial Randomness) and Berman's Z_2 statistics were used to test the strength of evidence for a covariate effect. The Receiver Operating Characteristic (ROC) plot, and the area under the ROC curve (AUC), closely related to Berman's Z_2 test, measure the magnitude of the covariate effect. AUC values close to 1 or 0 indicate strong discrimination, whereas intermediate values (0.5) suggest no discrimination power.

Intensity, evaluated by means of kernel density maps, although informative and widespread in the literature, nonetheless does not provide sufficient information to reliably infer about site formation processes.

Whereas intensity is a first-order property of the point process, multiscale inter-point interaction is measured by second or higher-order moment quantities, such as the Ripley's K correlation function (Ripley, 1976, 1977) and the distance G -, F - and J -functions. Three different types of inter-point interaction are possible: random, regular or cluster. In a hypothesis-testing framework, point-wise envelopes are computed by a number of random simulations of the null hypothesis (i.e., random/Poisson distribution). Thus, values of the empirical distribution (black solid line) are plotted against the benchmark value (red dotted line) and the envelopes (grey area) which specify the critical points for a Monte Carlo test (Ripley, 1981). Regular patterns are assumed to be the result of inhibition processes, while cluster patterns are the result of attraction processes.

In order to test the spatial interaction between remains associated with the erosional event of UB4c and those associated with the underlying UB5a unit, we treated the data as a multivariate point pattern, assuming that the point patterns in UB4c and UB5a are expressions of two different stationary point processes, i.e., depositional events. We performed a cross-type pair correlation function ($g_{ij}(r)$), derivative of the multitype $K_{ij}(r)$ function, which is the expected number of points of type j lying at a distance r of a typical point of type i . The function is a multiscale measurement of the spatial dependence between types i (UB4c) and j (UB5a). Randomly shifting in 199 Monte Carlo permutations each of the two patterns, independently of each other, estimated values of $\hat{g}_{ij}(r)$ are compared to a benchmark value $g_{ij}(r) = 1$, which is consistent with independence or at least with lack of correlation between the two point processes.

In addition to the pair correlation function, the multitype nearest-neighbour $G_{ij}(r)$ function was used to estimate the cumulative distribution of the distance from a point of type i (UB4c) to the nearest point of type j (UB5a). It measures the spatial association between the two assemblages. For the cross-type G -function, the null hypothesis states that the points of type j follow a Poisson (random) distribution in addition to being independent of the points of type i .

Thus, in a randomisation technique, when the solid line of the observed distribution ($\hat{G}_{ij}(r)$ or \hat{g}_{ij}) is above or below the shaded grey area, the pattern is significantly consistent with clustering or segregation, respectively. In order to reduce the edge effect bias in estimating the correlation between points, we implemented Ripley's isotropic edge correction (Ohser, 1983; Ripley, 1988).

Complete spatial randomness and independence (CSRI) of the two point processes (UB4c and UB5a) would support an allochthonous origin hypothesis for the assemblage recovered from the UB4c unit. According to the allochthonous model, the massive, chaotic UB4c flow event randomly re-elaborated the material entrained in it, inde-

Table 3: Value and p – value of circular uniformity test statistics.

| Sample | mean dir. | Rayleigh | | Kuiper | | Watson | | Rao | |
|--------------------|-----------|----------|-----------|----------------|------------------|----------------|------------------|----------|--------|
| | | R | p | V _n | p | U ² | p | U | p |
| UA3c | 77.17° | 0.268 | 0.029 | 2.4698 | <0.01 | 0.2967 | <0.01 | 271.8367 | <0.001 |
| UA4 | 35.79° | 0.386 | 0.003 | 2.5656 | <0.01 | 0.3437 | <0.01 | 246.3158 | <0.001 |
| <i>P. antiquus</i> | 54.64° | 0.489 | 2.775e-07 | 3.4811 | <0.01 | 0.906 | <0.01 | 291.4286 | <0.001 |
| UB4c (clock) | 91.66° | 0.276 | 0.054 | 1.8963 | 0.01< p <0.025 | 0.1937 | 0.025< p <0.05 | 255.7895 | <0.001 |
| UB4c (compass) | 151.17° | 0.243 | 0.106 | 1.3944 | >0.15 | 0.1268 | >0.10 | 128.5263 | >0.10 |

385 pendently from the material deposited in UB5a. On the other hand, positive or negative
 386 association can be interpreted as expressions of different autochthonous processes.

387 As for the three-dimensional distribution of the lithic artefacts in Area A, and
 388 their spatial association with the partial skeleton of the *P. antiquus*, we applied three-
 389 dimensional univariate and bivariate second-order functions. A rectangular box of 20
 390 square meters and 80 cm vertical extent was selected for the analyses (green outline in
 391 Fig. 11a). Assuming homogeneity, the univariate pair correlation function ($g_3(r)$) was
 392 estimated for the pattern of all the artefacts (mostly debris/chips) from UA3c and UA4.

393 In the specific context of the site, complete spatial randomness (CSR) would sug-
 394 gest that the pattern most probably is the result of a random distribution process, such
 395 as a high energy mass movement, thus supporting an allochthonous model of depo-
 396 sition. On the other hand, spatial aggregation would support a primary origin of the
 397 assemblage. Nevertheless, topography and natural obstructions may generate spatial
 398 clustering as well.

399 In support to the pair correlation function, the cross-type nearest-neighbour func-
 400 tion has been applied in order to compute, for each artefact recovered from the UA3c
 401 and UA4 units, the nearest point of the three-dimensional clouds of points associated
 402 with the elephant skeleton. A prevalence of short distances would indicate aggregation
 403 of the lithic artefacts around the mass of the elephant; whereas a uniform or symmetric
 404 distribution would support the action of random independent processes

405 3. Results

406 3.1. Fabric analysis

407 The rose diagrams in Fig. 6 visualise the circular distributions of the examined
 408 specimens. Overall, the UA4 sample and the sample of elephant bones show uni-
 409 modal distributions with predominant peaks in the NE quadrant; while the ones from
 410 units UA3c and UB4c suggest multimodal distributions. Specifically, the UA4 sample
 411 distribution (Fig. 6b) spreads largely in the NE quadrant. Similarly, the circular dis-
 412 tribution of the elephant sample (Fig. 6c), mainly lying in UA4, resembles the former
 413 distribution: it is skewed to the SW and concentrated in the NE quadrant. On the other
 414 hand, the UA3c sample (Fig. 6a) shows a bimodal distribution with two peaks to the E
 415 and NE, and the two samples from Area B (Fig. 6d,e) suggest a different multimodal
 416 scenario uniformly distributed.

417 Table 3 summarises the results of the circular uniformity tests. With regard to the
 418 UA3c sample, the Rayleigh test (p – value = 0.03) rejected the null hypothesis of cir-
 419 cular uniformity. The mean resultant length (\bar{R} = 0.27) and the mean direction of 77°

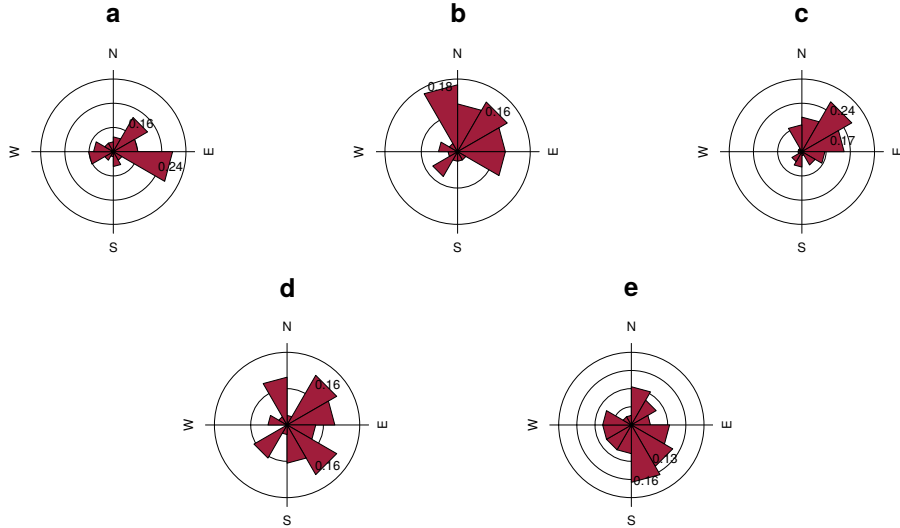


Figure 6: Rose diagrams showing the bearing patterns of samples from UA3c (a), UA4 (b), the elephant carcass (c) and UB4c (d: clock method, e: compass method).

are thus significant, assuming the distribution is unimodal. However, the rose diagram (Fig. 6a) showed a bimodal distribution. The Kuiper, Watson and Rao omnibus tests, more powerful than the Rayleigh test in detecting multimodal deviation from uniformity, also rejected the null hypothesis of uniformity, therefore suggesting significant anisotropy in the distribution.

For the UA4 sample and the subset of elephant bones, all the uniformity tests agreed in rejecting the null hypothesis in favour of a preferentially oriented distribution. The elephant sample, with respect to the other, showed significantly higher test results, thus stronger anisotropy. As suggested by the rose diagrams (Fig. 6c), this sample has a mean direction towards the NE (55°) and relatively low circular variance (29°).

The UB4c sub-samples had discordant test results when considering the omnibus statistics. However, according to the Rayleigh test, the mean resultant lengths (\bar{R}) and the mean directions were not significant for both sub-samples of measurements: $p - values > 0.05$ failed to reject the null hypothesis of isotropy with 95% confidence interval. This result is well confirmed by the Kuiper, Watson and Rao tests for the sub-sample of measurements recorded using the compass. Conversely, the omnibus tests failed to reject the hypothesis of uniformity for the other sub-sample of measurements recorded with the clock method. The rose diagram (Fig. 6d) suggested for the latter distribution strong multimodality, with uniformly spread peaks. The contrasting results obtained for the UB4c sub-samples are most probably due to the shape of those distributions. Indeed, the clock system, being less accurate, tends to produce a less dense distribution, more subject to show a multimodal shape when the distribution is actually uniform (Fig. 6a,d).

The Woodcock eigenvalues ratio graph (Fig. 7a) presents the shape (K) and strength

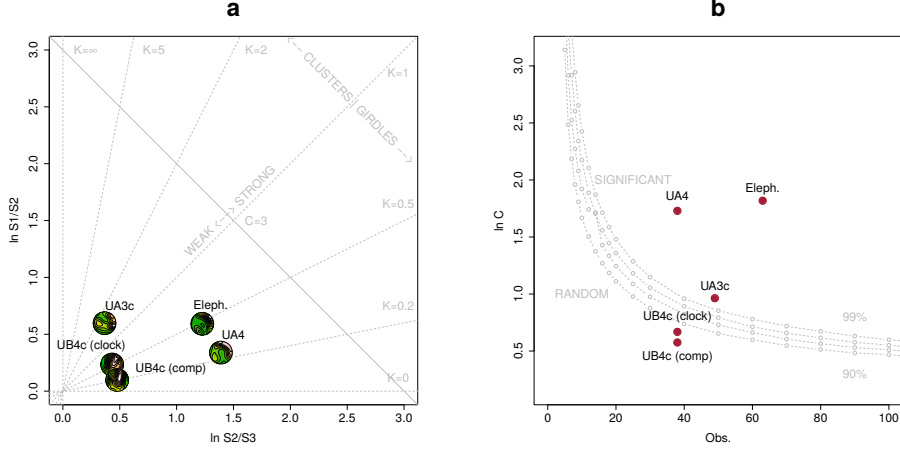


Figure 7: Woodcock's eigenvalues ratio graph (a) and plot of the Monte-Carlo critical S_1/S_3 test values, for varying sample sizes and confidence levels (b), modified from [Woodcock and Naylor \(1983\)](#).

(C) of the distributions. Fig. 7b plots confidence levels of Monte-Carlo critical C values, varying for sample sizes. The two sub-samples from Area B nearly overlapped, thus suggesting reliability of the orientation measurements collected using the clock system, although of low accuracy. The two sub-samples, together with the UA3c sample, having low C values, plotted close to the origin of the ratio graph. Therefore, they indicate weak preferential orientation (UA3c) and significant randomness (UB4c). On the other hand, the UA4 and the elephant samples, with higher C values, showed a stronger and significant tendency to orient preferentially. The shape parameter K of the samples varied from $K = 0.25$ for the UB4c sample measured with the compass, to $K = 0.66$ for the one measured with the clock, to $K = 0.48$ for the elephant sample. Overall, all the samples, except the UA3c one ($K = 1.63$), plotted below the average shape value ($K = 1$) between girdles and clusters distributions.

The Benn diagram (Fig. 8) resembles the Woodcock ratio graph (Fig. 7a). The samples from units UB4c and UA3c clearly plotted at a distance from the UA4 and the elephant samples. The UB4c samples plotted in the upper corner of the ternary graph, with the UB4c sub-sample of measurements taken with the compass exhibiting more isotropy. The UA3c sample, with an elongation index similar to the elephant sample, but higher isotropic index, plotted towards the centre. Compared to the ranges of fabrics recorded for modern natural processes (debris flow and runoff), the fabric from the UA3c and UB4c units plotted well inside the cluster of debris flows, with the UB4c (comp) sample suggesting even more random orientations. On the other hand, the sample of elephant remains, which lie mostly on UA4 and are covered by UA3c, plotted significantly close to the sample from unit UA4. They both presented the lowest isotropy index (IS), but not high elongation index (EL). Thus, they plotted in the average between linear and planar orientations, at the margins of the range of runoff processes. Yet they still plotted within the cluster of debris flows fabrics. Moreover, as suggested also by the uniformity tests (Tab. 3), the elephant sample showed a more

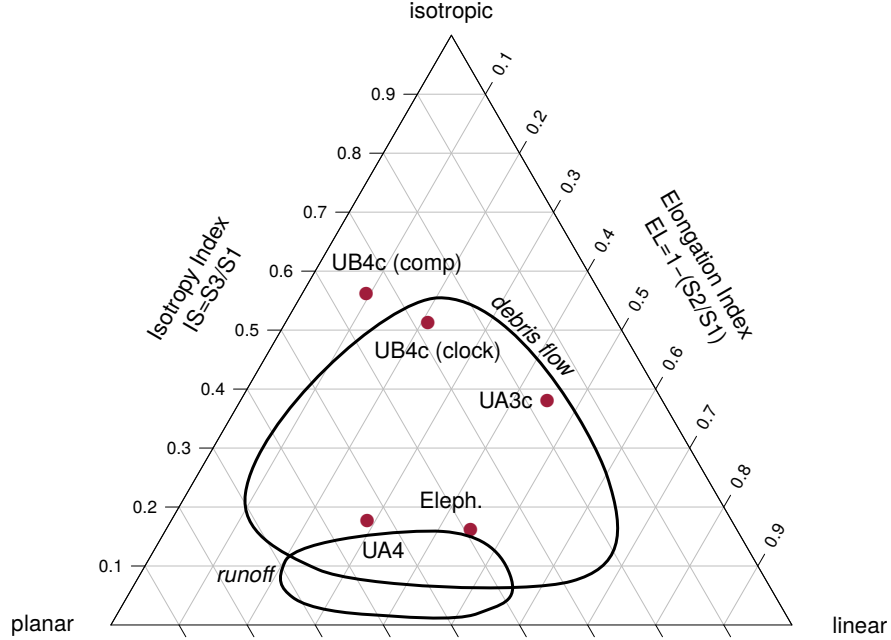


Figure 8: Benn's diagram. Fabric ranges of natural processes modified from [Lenoble and Bertran \(2004\)](#).

471 linear attitude with respect to the UA4 sample.

472 **3.2. Vertical distribution**

473 Fig. 9 compares the vertical distribution of the finds from units UA3c and UA4, by
 474 means of empirical density functions of the minimum distances (d) from each speci-
 475 men to the UA3c/4 erosional contact (Fig. 5a). Three lithic artefacts (two flakes and
 476 one tool) from the UA3c unit, not included in Fig. 9, plotted within 15 cm from the
 477 interpolated surface. Only one flake has been found in the lower UA4, at about 17 cm
 478 from the UA3c/4 contact, together with three chips. Despite the scarcity of debitage
 479 products in this area, waste products (debris/chip) are relatively well represented (16%
 480 of the UA3c sample). Their vertical dispersion approximated a normal distribution
 481 ($\mu = 0.24$, $\sigma = 0.15$): the Kolmogorov-Smirnov and Shapiro tests failed to rejected
 482 the null hypothesis of normality ($p - value = 0.83$ and 0.075, respectively). Notably, the
 483 distributions of the faunal remains from the same unit UA3c were all right skewed, with
 484 means (μ) about 20 cm above the UA3c/4 contact. Nevertheless, the Welch two sample
 485 t-test ($p - value = 0.61$) failed to reject the null hypothesis that the lithic and faunal
 486 sample means are equal. The total distribution of remains from unit UA3c showed a
 487 unimodal distribution, skewed to the right, with mode in the proximity of the UA3c/4
 488 surface. Similarly, the vertical distribution of faunal remains recovered from unit UA4
 489 concentrate in the first 10 cm below surface. The density functions altogether clearly
 490 confirmed one of the main observations assessed during excavation, namely that, with

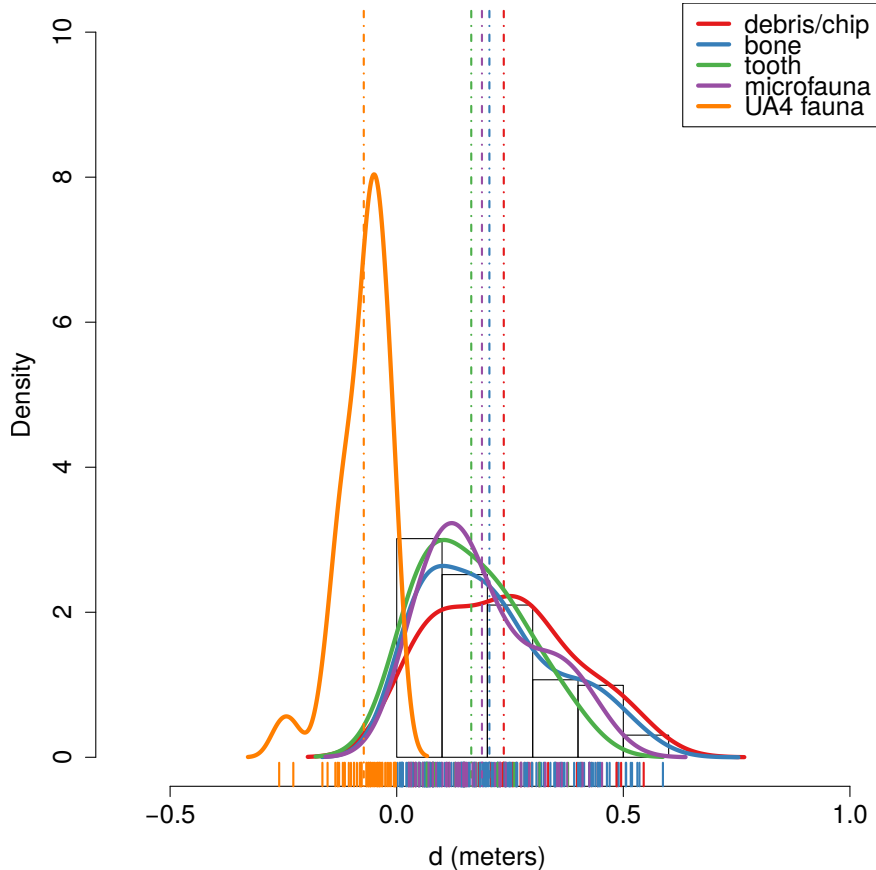


Figure 9: Empirical density functions of minimum orthogonal distances (d) to the UA3c/4 surface. The histogram represents the total distribution of remains from UA3c; dashed lines indicate mean values.

491 the elephant remains lying at the UA3c/4 contact and covered by unit UA3c, most of
 492 the faunal and lithic material were recovered from unit UA3c and predominantly in the
 493 proximity of the UA3c/4 contact.

494 Fig. 10 shows the empirical density functions of the minimum distances from each
 495 specimen from Area B to the UB4c/5a erosional contact (Fig. 5b). The combined
 496 distribution of any type of find from the UB5a unit (Fig. 10a) skewed to the left with
 497 a short tail (up to -0.3 m). The mode, between 5 and 10 cm below the roof of UB5a,
 498 indicates a general concentration of material very close to the contact of this unit with
 499 the overlying UB4c, in accordance with the mean distribution of the different classes of
 500 remains. Although the majority of both the lithic and faunal assemblages were found
 501 in the uppermost 15 cm of UB5a, few debris/chips and bone fragments occur lower
 502 in the sequence, yet no more than 30 cm below the roof of this unit. Very few flakes,
 503 three tools and no cores have been found in this unit. As a whole, the lithic assemblage

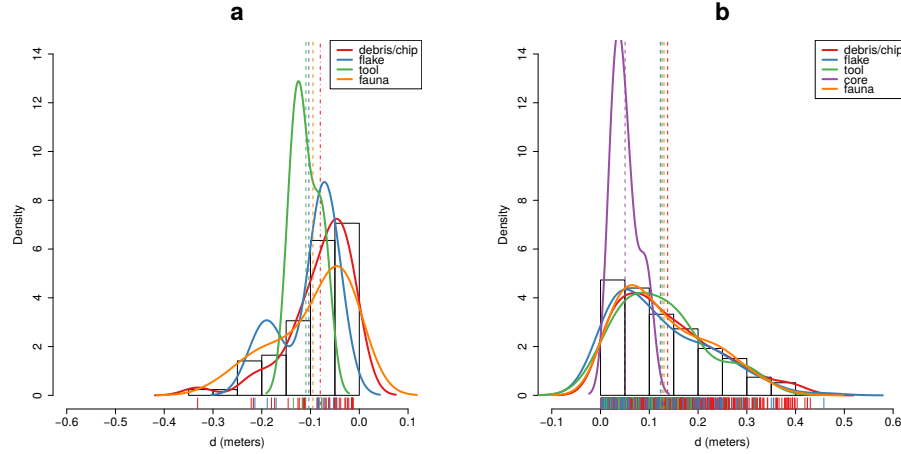


Figure 10: Empirical density functions of minimum orthogonal distances (d) to the UB4c/5a surface. The histogram represents the total distribution of remains from UB5a (a) and UB4c (b); dashed lines indicate mean values.

504 from UB5a, mostly composed by debris/chips, is only 7% of the most conspicuous
505 assemblage from UB4c.

506 The global distribution of unit UB4c was right skewed (up to almost 0.6 m) and
507 centred at about 5 cm above the contact with the underlying unit UB5a (Fig. 10b).
508 Almost 30% of the sample fell exactly at the erosional contact that separates UB4c
509 from UB5a. The density estimations of the lithic debris/chip, flakes, tools and faunal
510 remains significantly overlap, whereas the distribution of the six cores shows a bimodal
511 shape with peaks at 5 and 20 cm above the contact. Moreover, the Welch Two Sample t-
512 test of the lithic and faunal sample means failed to reject the null hypothesis (p -value =
513 0.6295).

514 3.3. Point pattern analysis

515 Results of the point pattern analysis are complementary to those obtained from the
516 analysis of the fabric and vertical distributions.

517 Regarding Area A, kernel density estimation and three-dimensional functions were
518 applied in order to quantitatively depict the spatial distribution of the lithic assemblage
519 in relation to the elephant skeleton.

520 Fig. 11a shows the smoothing kernel intensity estimation of the faunal assemblage
521 from the UA3c unit. Contour lines delimit the density of the lithic sample. The partial
522 skeleton of the *P. antiquus* is superimposed on it. A preliminary visual examination
523 of the plot suggests a homogeneous distribution of lithics (mostly debris/chips) and
524 fossils. Spots of higher density appear to be spread around and in association with the
525 elephant remains.

526 The univariate pair correlation function of the joined lithic assemblage from the
527 UA3c and UA4 units (Fig. 11b) suggests aggregation of finds. The estimated $\hat{g}_3(r)$
528 function (black solid line) wanders above the benchmark value (red dotted line) until

values of $r = 0.8$. However, for distances between 35 and 65 cm, it lies above the grey envelope of significance for the null hypothesis of CSR, indicating that at those distances artefacts occur significantly closer than expected in the case of random processes. For values of $r > 0.8$, the function stabilises at values close to 0, suggesting a Poisson distribution. The plot illustrates the random distribution of finds between patches of clusters that we observe in Fig. 11a.

The histogram in Fig. 11c shows the density of the distances calculated from each artefact to the nearest-neighbour elephant remain. A right skewed distribution, with a prevalent peak at 10 cm and mean (μ) 30 cm is an indication of the relatively strong aggregation of lithics around the mass of the elephant skeleton.

As for Area B, the analysis focused on the spatial distribution and cross-correlation of the assemblages from UB4c and UB5a (Fig. 12).

Figs. 12a,b respectively show kernel density estimations of the combined lithic and faunal assemblages from both the units analysed. Despite the samples size difference, a first visual examination suggests the presence of interesting spatial structures.

Regarding the UB4c unit (Fig. 12a), the high density of material concentrated around the western square 934/600 suggests that the pattern could have been the result of an inhomogeneous, non-uniform depositional process. Visual comparison of the density plot with the elevation model of the erosional contact between the UB4c and UB5a units (Fig. 5b) suggests positive correlation between lower elevations (topographic depressions) and higher density of remains. Fig. 12c shows the results of the ρ -function, which estimates the intensity of the UB4c sample assemblage as a function of the covariate underlying topography created by the erosional event. Within the range of elevation between 350.2 and 350.4 m, the occurrence of finds is higher and the intensity decreases with the rise of elevation, i.e., finds are more likely to be found at lower elevations than would be expected if the intensity was constant.

Spatial Kolmogorov-Smirnov (KS) and Berman's Z_2 (Berman, 1986) statistics were used in order to test the dependence of the UB4c pattern on the covariate erosional surface. Both KS ($D = 0.11952$, $p - value = 7.772e - 16$) and Z_2 ($Z_2 = -7.8447$, $p - value = 4.34e - 15$) significantly rejected the null hypothesis of CSR. Although the tests suggested evidence that the intensity depends on the covariate, the effect of the covariate is weak and it seems to have no discriminatory power. The ROC curve and AUC statistics (0.56), which measure the strength of the covariate effect, suggest that the underlying UB4c/5a topography does not completely explain the localised high density of occurrence in the UB4c.

Relative spatial segregation seems to occur between the assemblages from UB4c (Fig. 12a) and UB5a (Fig. 12b), with high density of the former distribution corresponding to low density of the latter. The former analysis of the vertical distribution showed that the two assemblages occur very close to their stratigraphic contact. In order to further investigate the spatial interaction between the two depositional events, we applied multitype pair correlation ($g_{ij}(r)$) and nearest-neighbour ($G_{ij}(r)$) functions.

Fig. 12d shows the estimated values of the multivariate $\hat{g}_{ij}(r)$ function against the envelope of the null hypothesis, obtained by randomly shifting the position of remains from the two distributions in 199 Monte Carlo simulations. For fixed values of r less than 30 cm the observed function lies below the benchmark value of independence, thus indicating segregation; but it wanders at the lower edge of the grey envelope. For fixed

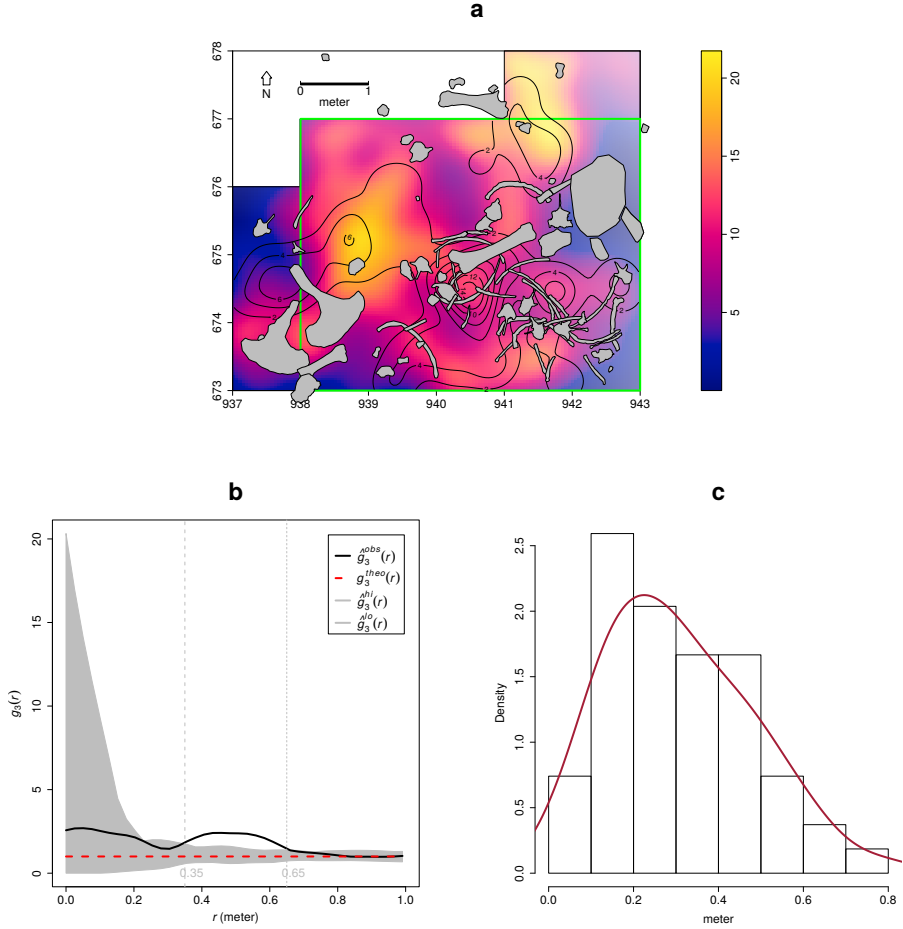


Figure 11: Kernel smoothed intensity function of the faunal assemblages from UA3c. Isolines mark the density of the lithic artefacts from UA3c (a). Pair correlation function ($g_3(r)$) of a three-dimensional pattern of lithic artefacts from UA3c and UA4. Grey envelope of 999 Monte Carlo simulations under the CSR null hypothesis (b). Three-dimensional distance from each lithic artefact from UA3c and UA4 to the nearest neighbour elephant remain (c).

575 distances of $r > 0.3$ m the observed and theoretical lines significantly overlap. Overall,
576 the function suggests independence of the two point processes (UB4c and UB5a) at
577 multiple scales.

578 However, the estimated $\hat{G}_{ij}(r)$ function (Fig. 12c), running well below the signifi-
579 cence grey envelope for fixed values of $r > 0.3$ m, confirms that the nearest-neighbour
580 distances between remains from UB4c and UB5a are significantly longer than expected
581 in the case of independent processes. Interestingly, at values of $r < 0.2$ m the observed
582 function failed to reject the null hypothesis of Complete Spatial Randomness and In-
583 dependence (CSRI).

584 4. Discussion

585 Recent excavations at the Middle Pleistocene site of Marathousa 1 have unearthed
586 in one of the two investigated areas (Area A) a partial skeleton of a single individual
587 of *Palaeoloxodon antiquus*, whose bones are in close anatomical association, and spa-
588 tially and stratigraphically associated with lithic artefacts and other faunal remains. In
589 Area B, 60 m to the South of Area A, we collected a much higher number of lithic
590 artefacts (Tourloukis et al., this issue), spatially and stratigraphically associated with
591 other faunal remains, including isolated elephant bones, cervids and carnivores among
592 others (Konidaris et al., this issue).

593 The two areas are stratigraphically correlated, the main fossiliferous layers (UA3c
594 and UB4c) representing a massive depositional process, such as a hyperconcentrated
595 flow that dumped material in a lake margin context (Karkanas et al., this issue).

596 To date, evidence of butchering (cut-marks) has been identified on two bones of
597 the elephant skeleton from Area A, as well on elephant and other mammal bones from
598 Area B (see Konidaris et al. (this issue)).

599 However, due to the secondary depositional nature of the main fossiliferous hori-
600 zon, it is of primary importance to evaluate the degree and reliability of the spatial
601 association of the lithic artefacts with the faunal remains, and especially with the ele-
602 phant skeleton. In order to tackle our main objective, we applied a comprehensive
603 set of spatial statistics to the distributions of the archaeological and zooarchaeologi-
604 cal/palaeontological remains from relevant stratigraphic units of the two areas of in-
605 vestigation. Preliminary results of our analyses are here discussed for both areas.

606 4.1. Fabric analysis

607 The analysis of the orientation (plunge and bearing) of subsets of remains, mostly
608 bone, wood fragments and lithic artefacts, showed different patterns for the two main
609 find-bearing units.

610 In Area B, two sub-samples from the same stratigraphic unit were analysed, in order
611 to asses the reliability of the orientation data measured with the clock system. Due to
612 the different shapes of the distributions (Figs. 6d,e), test statistics reported contrasting
613 results (Tab. 3). Indeed, the clock system, recording non-continuous circular data,
614 tends to produce a distribution more subject to show a multimodal shape when it is
615 actually uniform. However, the two sub-samples nearly overlapped when plotted in
616 the three-dimensional Woodcock (Fig. 7) and Benn (Fig. 8) diagrams, thus suggesting

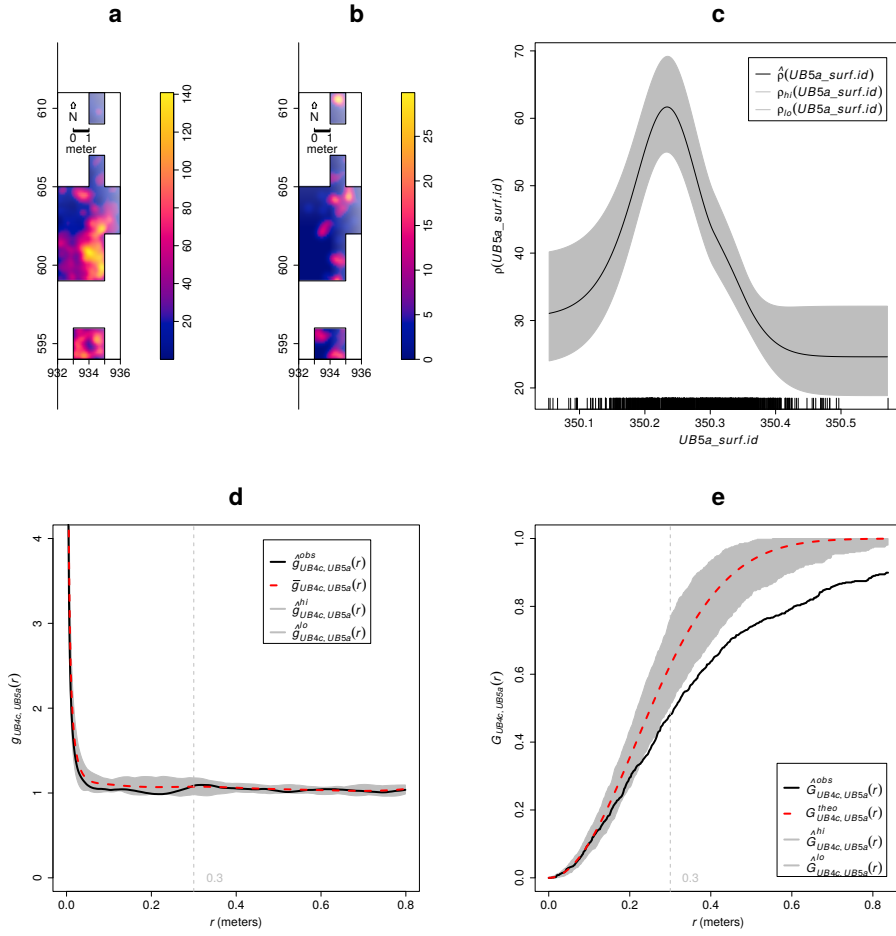


Figure 12: Kernel smoothed intensity function of the lithic and faunal assemblages from UB4c (a) and UB5a (b). Smoothing estimate of the intensity of remains from UB4c, as a function of the erosional surface UB4c/5a. Grey shading is point-wise 95% confidence bands (c). Cross-pattern pair correlation function ($g_{ij}(r)$) between the UB4c and UB5a distributions. Grey envelope of 199 Monte Carlo simulations under the independence of components null hypothesis (d). Multitype nearest-neighbour function ($G_{ij}(r)$) between the UB4c and UB5a distributions (e).

617 some degree of reliability of the clock method. Nevertheless, despite minor differences
618 between the two samples, caution should be paid in analysing grouped circular data.

619 The test results (Tab. 3) for the UA4 sample and the sample of elephant remains
620 - which lie on unit UA4 and are covered by UA3c - indicated significant preferential
621 orientations towards the NE (Figs. 6b,c). As shown by the Woodcock's (Fig. 7) and the
622 Benn's diagrams (Fig. 8), these samples plotted together at a distance from the others.
623 Such convergence suggests that the elephant carcass, the other faunal remains and the
624 organic material, deposited on unit UA4, were subject to the same processes.

625 Far from the isotropic corner in the Benn's diagram these two samples from Area
626 A plotted approximately in between the linear and planar extremes, with the elephant
627 sample showing a more linear fabric. When the results published by Bertran et al.
628 (1997) and Lenoble and Bertran (2004) from observations of fabrics in modern sub-
629 aereal slope deposits were used as a reference, the two samples aggregated at the ex-
630 treme margins of runoff processes. Yet, they plotted well within the cluster of debris
631 flows and relatively distant from the linear corner.

632 Although Bertran et al. (1997) studied runoff deposits from different environments
633 (channel-lag gravels in rills, small gullies, and inter-rill surfaces on alpine slopes; and
634 faintly laminated gravel lenses on an inactive, small colluvial fan), this result is consis-
635 tent with the exposure of unit UA4 to overland water-laden processes that occurred be-
636 fore the flood event UA3c/UB4c. Notably, the erosive nature of low-energy processes
637 triggered by rain-water has been observed on lacustrine floodplains, and is associated
638 with anisotropic patterns in autochthonous assemblages (Cobo-Sánchez et al., 2014;
639 Domínguez-Rodrigo et al., 2014c; García-Moreno et al., 2016).

640 Pockets of thinly bedded organic-rich silty sands have been found mixed in UA4.
641 These sands in Area A resemble the UB5b/c sandy deposit in Area B, which is associ-
642 ated with relatively high energy fluvial flows entering the lake margins (Karkanas et al.,
643 this issue). Eventually, such relatively high energy flood (UB5b/c) would have had the
644 power to significantly reorient elements of the elephant carcass and slightly displace
645 them. However, the elephant skeleton clearly lies on top of unit UA4 and is covered by
646 UA3c (see Fig.4 and SI).

647 Moreover, unlike bones with a tubular shape (i.e., long bones), ribs and vertebrae
648 are prone to orient preferentially under high energy processes, less likely under low
649 energy processes (Domínguez-Rodrigo and García-Pérez, 2013; Domínguez-Rodrigo
650 et al., 2014c). Interestingly, whereas some of the ribs share the same preferential orien-
651 tation with the long bones, others are oriented NW/SE. However, a NW/SE orientation
652 could be consistent with a prevalent NE direction of the flow (and vice-versa), since
653 long bones could roll orthogonally to the flow direction (Voorhies, 1969). On the other
654 hand, a higher energy flood would lead to an under-representation of carpals, tarsals,
655 metapodials, phalanges, ribs and vertebrae, which are more prone - when disarticulated
656 - to be easily transported by water induced processes (Voorhies, 1969). Yet, several of
657 these bones are present and in close spatial association with the elephant cranium and
658 other skeletal elements. The presence of many of the skeletal elements with different
659 transportation properties suggests that the elephant carcass was not subjected to high
660 energy processes before the flood event UA3c/UB4c.

661 The fabrics of the UA3c and UB4c samples, with higher isotropic index (*IS*), plot-
662 ted at a significant distance from the elephant sample, yet within the cluster of debris

flows (Fig. 8). Indeed, random distribution and orientation of clasts is expected for debris flows, except at flow margins, where preferential orientation and clusters of clasts have been observed (Pierson, 2005). However, hyperconcentrated flows, such as the UA3c/UB4c flood event, which fall in between the spectrum of water and debris flows, may develop parallel or normal orientation to the flow direction (Lindsay, 1968; Benvenuti and Martini, 2002). Notably, with respect to the UB4c sample, the UA3c sample exhibits a higher elongation index (ES), similar to that of the elephant sample (Fig. 8). Rose diagrams (Fig. 6) and uniformity tests (Tab. 3) also suggest similar fabrics of the samples from Area A.

Thus, we can assume that an overland flow, namely UA3c/UB4c, is likely to have slightly reworked and preferentially oriented to the NE the exposed elements of the already dismembered (and probably already marginally displaced) elephant carcass, which mostly preserves close anatomical associations, but not anatomical connections.

Although little is currently known about the spatial extension of the UA3c/UB4c flow event, the different orientation patterns between the two areas could probably be explained with lateral variability. Indeed, the same event could exhibit different behaviours at different temporal and spatial points, giving rise to different distribution patterns.

As suggested by Lenoble and Bertran (2004), fabric analysis is not sufficient to unequivocally discriminate processes and should therefore be integrated with the analysis of other diagnostic features.

4.2. Vertical distribution

As for the vertical distribution, we assumed that mass processes, such as hyperconcentrated flows, would predominantly distribute poor to very poor sorted clasts homogeneously throughout the sequence (Pierson, 2005). Diagnostic inverse grading, or a continuously aggrading bed can be observed in the resultant deposits (Benvenuti and Martini, 2002). A concentration of unsorted elements in the proximity of the erosional surface, as well as the absence of any grading, would in turn suggest an autochthonous assemblage.

The lithic assemblage from Area A - the combined units UA3c and UA4 ($n = 54$), composed by a few debitage products and a relatively high number of debris/chips and retouch waste products (Tab. 2) - plotted predominantly in the proximity of the erosional surface created by the UA3c/UB4c event (Fig. 5a). The faunal remains from unit UA3c resemble the distribution of the archaeological assemblage; whereas the ones from the underlying unit UA4 plotted within 10 cm below the erosional contact. Overall, the material recovered from unit UA3c did not show any grading and mainly plotted at the bottom of the unit (Fig. 9). Thus, its vertical distribution is consistent with the hypothesis of an autochthonous assemblage.

In Area B, two samples from units UB4c ($n = 1243$) and UB5a ($n = 101$) respectively, were analysed (Tab. 2) for quantifying the minimum orthogonal distance of each item to the modelled erosional surface (Fig. 5b).

The vertical distribution of lithic artefacts and fossils from unit UB4c showed a predominant peak right at the contact with the erosional surface. Almost 30% of this rich sample plotted at a distance between 0 and 5 cm from the erosional contact; whereas

707 the rest gently skewed to the upper part of the unit, up to about 50 cm. The same distribution
708 was observed for all classes of remains, suggesting no size sorting and an origin
709 very close to the erosional surface (Fig. 10b).

710 The density distribution of the sample from the underlying UB5a unit (Fig. 10a)
711 globally indicates a more constrained vertical displacement of remains (within 30 cm
712 below the erosional surface). Whereas lithic artefacts and fossils mostly plot right at
713 the contact and just below it, a few debris/chips and faunal remains were found lower
714 in the sequence. No size sorting was observed, but, notably, lithic cores are absent and
715 the debris/chip distribution is wider than the distribution of the few flakes and tools.

716 Field observations of cracks in the clayey UB5a unit testify to shrinking and swelling
717 during wet and dry cycles (Karkanas et al., this issue), which suggests that vertical dis-
718 placement of some small lithics and fossil fragments at lower depths with respect to
719 the UB5a/4c contact probably resulted from clay desiccation.

720 Likewise, Lenoble and Bertran (2004) documented up to 30 cm vertical dispersion
721 and frequent vertical plunge of artefacts from the marshy silty clay of the Croix-de-
722 Canard site, sector 3. Furthermore, a recent experimental study of animal trampling
723 in water saturated substrates reported negative correlation with artefact size, signifi-
724 cant inclination and greater vertical displacement than any former work: a maximum
725 between 16 and 21 cm, with a mean of about 6 cm (Eren et al., 2010).

726 The fact that the majority of the remains from units UB4c and UB5a plotted at, or
727 very close to the contact between these two layers, the relatively high percentage of
728 lithics in both units, as well as the absence of grading, suggest autochthonous assem-
729 blages, deposited in UB5a and subsequently eroded *in situ* by the UA3c/UB4c flood
730 event.

731 4.3. Point pattern analysis

732 The autochthonous hypothesis was further explored by means of point pattern
733 analysis. According to this model, in both areas the lithic and faunal assemblages
734 were primarily deposited *in situ* and were subsequently eroded and re-deposited (*sensu*
735 Fernández-López, 1991) by the hyperconcentrated flow UA3c/UB4c. We assumed
736 that a completely random spatial distribution of the lithic artefacts and faunal remains
737 would suggest an allochthonous origin and subsequent re-elaboration (*sensu* Fernández-
738 López, 1991), with transport to the site by the action of a random massive process.
739 Nevertheless, clustering of artefacts is not necessarily evidence of human presence.
740 Aggregation or segregation patterns could be produced by a range of biotic and/or nat-
741 ural processes. Human activities, topography and physical obstructions alike could
742 trigger spatial aggregation.

743 The three-dimensional distribution of lithic artefacts from unit UA3c shows signif-
744 icant clustering for values of r between 35 and 65 cm. Lithic artefacts occur relatively
745 close to the skeletal elements of the elephant, at a distance between 20 and 50 cm at
746 most (Fig. 11). The richest cluster of about 20 lithic artefacts is located to the SW of
747 the cranium, close to the right femur and the scatter of ribs and vertebrae.

748 Considering the prevalent NE orientation of the elephant bones and the other fau-
749 nal remains from UA4 and UA3c, it is not unlikely that a SW/NE oriented flood could
750 have been responsible for the observed accumulation to the SW of the elephant cra-
751 nium, which would have represented an important obstruction to the flow. A similar

752 case of clustering of small remains, apparently dammed by a long elephant tusk, has
753 also been observed at Castel di Guido (Italy) (Boschian and Saccà, 2010). Secondary
754 deposition by low-energy flows and clustering of artefacts and bones blocked by an
755 aurochs carcass have been as well documented at the site of 'Ein Qashishadd (Israel)
756 (Hovers et al., 2014).

757 However, the pair correlation function (Fig. 9b) suggests significant clustering of
758 lithic artefacts at relatively small scale: a pattern less likely to be produced by a large
759 scale massive process such as a hyperconcentrated flow. Moreover, clusters of lithic
760 artefacts occur as well in areas with lower densities of elephant bones.

761 Small scale clustering; proximity to the elephant remains and the erosional sur-
762 face; absence of spatial size sorting and, on the contrary, the presence of a relatively
763 high number of lithic debris/chips associated with some flakes, tools and a rich fau-
764 nal assemblage; close anatomical spatial association of the elephant skeletal elements,
765 slightly displaced and preferentially oriented: altogether these lines of evidence support
766 the hypothesis of an autochthonous deposition, subject to localised minor reworking.

767 A similar pattern can be observed in Area B, where an initial set of spatial statistics
768 confirmed that the inhomogeneous density of remains from unit UB4c (Fig. 12a) is
769 not completely explained by the covariate effect of the underlying complex topography
770 created by the erosional event UA3c/UB4c (Fig. 5b).

771 Thus, we explored the relative spatial interaction between the UB4c and the un-
772 derlying UB5a samples. We assumed that complete spatial randomness of the two
773 independent depositional processes would occur in case of an allochthonous origin and
774 transportation of the UB4c assemblage. The hypothesis of an autochthonous original
775 deposition of the faunal and lithic assemblages on the UB5a unit, subsequently eroded
776 *in situ* by a relatively high energy flood (UB4c), was tested by cross-pattern spatial
777 correlation functions (Figs. 12d,e). Whereas the two samples are vertically adjacent to
778 the erosional surface (Fig. 10), on the horizontal plane they are both more segregated
779 than expected for a random distribution.

780 Conversely, the extraordinary preservation and number of mint to sharp, unsorted
781 lithic artefacts from the UB4c unit; their density, positively correlated to the topog-
782 raphy, and significantly segregated from the underlying distribution of remains; the
783 vertical proximity of both assemblages from UB4c and UB5a to the erosional surface;
784 as well as the random orientation pattern of the former, suggest that significant dis-
785 placement of materials due to the erosional event can be excluded.

786 The faunal and lithic assemblages from unit UB4c therefore most likely derived
787 from the local erosion of exposed mudflat areas (unit UB5a) and have been slightly
788 redistributed by the same flood event that capped the elephant in Area A.

789 Further evidence that the recovered assemblage has not undergone substantial re-
790 working and has retained its original characteristics would come from the refitting anal-
791 ysis, currently in progress. To date, 4 bone refits have been found in Area B: three from
792 unit UB4c, respectively at 4.77, 0.05 and 0.01 m distance; and one between two mam-
793 mal bone fragments from units UB4c and UB5a, at a very short distance (0.09 m).
794 Interestingly, one of the elements of the most distant refit (a *Dama* sp. mandibular
795 fragment) shows traces of carnivore gnawing (Konidaris et al., this issue).

796 In conclusion, multiple lines of evidence reject an allochthonous hypothesis of de-
797 position in favour of an autochthonous model. The erosional event UA3c/UB4c repre-

798 sents an *en masse* depositional process, i.e. a hyperconcentrated flow, in the continuum
799 between water and debris flow, which would have locally reworked at a small scale
800 the already exposed or slightly buried and spatially associated lithic and faunal assem-
801 blages.

802 Although the UA3c/UB4c process represents a snapshot of a relatively short time-
803 frame, high resolution inferences about the use of space by human groups, in terms
804 of knapping episodes and butchering activities, are unreliable in light of the current
805 information.

806 The spatial pattern observed at the site is indeed the result of the last episode in a
807 palimpsest of spatial processes. Whereas the erosional event represented by the hyper-
808 concentrated flow UA3c/UB4c caps the fossiliferous horizon and preserves the record,
809 little is known about the underlying, eroded 'occupational' surface.

810 However, whereas hunting or scavenging in the Lower Palaeolithic is still an un-
811 solved matter of debate, considering the rate of bone fragmentation, the density of lithic
812 debris/chips, the number of processed bones and their spatial density and association, it
813 is likely that the assemblage represents a complex palimpsest of locally repeated events
814 of hunting/scavenging and exploitation of lake shore resources.

815 More data from high resolution excavations in the coming years will allow us to
816 refine the coarse-grained spatio-temporal resolution of our inferences about past human
817 behaviour at Marathousa 1.

818 5. Conclusions

819 At the Middle Pleistocene open-air site of Marathousa 1, a partial skeleton of a
820 single individual of *Palaeoloxodon antiquus* was recovered in stratigraphic association
821 with a rich and consistent lithic assemblage and other vertebrate remains. Cut-marks
822 and percussion marks have been identified on the elephant and other mammal bones ex-
823 cavated at the site. The main find-bearing horizon represents a secondary depositional
824 process in a lake margin context.

825 Understanding the site formation processes is of primary importance in order to
826 reliably infer hominin exploitation of the elephant carcass and other animals. To meet
827 this aim, we applied a comprehensive set of multivariate and multiscale spatial analyses
828 in a taphonomic framework.

829 Results from the fabric, vertical distribution and point pattern analyses are consis-
830 tent with a relatively high-energy erosional process slightly reworking at a small scale
831 an exposed (or slightly buried) and consistent scatter of lithic artefacts and faunal re-
832 mains. These results are in agreement with preliminary taphonomic observations of the
833 lithic artefacts (Tourloukis et al., this issue) and the faunal remains (Konidaris et al.,
834 this issue), which also indicate minor weathering and transportation. Our analyses
835 show that multiple lines of evidence support an autochthonous origin of the lithic and
836 faunal assemblages, subject to minor post-depositional reworking.

837 Acknowledgements

838 This research is supported by the European Research Council (ERC StG PaGE
839 283503) awarded to K. Harvati. We are grateful to the Municipality of Megalopolis,

840 the authorities of the Region of Peloponnese, and the Greek Public Power corporation
841 (Δ EH) for their support. We also thank Julian Bega and all the participants in the
842 PaGE survey and excavation campaigns in Megalopolis for their indispensable coop-
843 eration. We are grateful to the editors and two anonymous reviewers for their critical
844 discussions and many constructive comments that helped to improve this manuscript.

845 **References**

- 846 Anderson, K. L., Burke, A., 2008. Refining the definition of cultural levels at Karabi
847 Tamchin: a quantitative approach to vertical intra-site spatial analysis. *Journal of*
848 *Archaeological Science* 35 (8), 2274–2285.
- 849 Aramendi, J., Uribelarrea, D., Arriaza, M. C., Arráiz, H., Barbón, D., Yravedra, J.,
850 Ortega, M. C., Gidna, A., Mabulla, A., Baquedano, E., Domínguez-Rodrigo, M.,
851 2017. The paleoecology and taphonomy of {AMK} (bed i, olduvai gorge) and its
852 contributions to the understanding of the “zinj” paleolandscape. *Palaeogeography,*
853 *Palaeoclimatology, Palaeoecology*, –.
- 854 Baddeley, A., Chang, Y.-M., Song, Y., Turner, R., 2012. Nonparametric estimation of
855 the dependence of a point process on spatial covariates. *Statistics and Its Interface*
856 5 (2), 221–236.
- 857 Bailey, G., 2007. Time perspectives, palimpsests and the archaeology of time. *Journal*
858 *of Anthropological Archaeology* 26 (2), 198 – 223.
- 859 Bar-Yosef, O., Tchernov, E., 1972. On the palaeo-ecological history of the site of Ubei-
860 diya. Vol. 35. Israel Academy of Sciences and Humanities, Jerusalem.
- 861 Bargalló, A., Gabucio, M. J., Rivals, F., 2016. Puzzling out a palimpsest: Testing an
862 interdisciplinary study in level o of abric romaní. *Quaternary International* 417 (Sup-
863 plement C), 51 – 65, advances in Palimpsest Dissection.
- 864 Benito-Calvo, A., de la Torre, I., 2011. Analysis of orientation patterns in Olduvai
865 Bed I assemblages using GIS techniques: Implications for site formation processes.
866 *Journal of Human Evolution* 61 (1), 50 – 60.
- 867 Benito-Calvo, A., Martínez-Moreno, J., Mora, R., Roy, M., Roda, X., 2011. Trampling
868 experiments at Cova Gran de Santa Linya, Pre-Pyrenees, Spain: their relevance for
869 archaeological fabrics of the Upper–Middle Paleolithic assemblages. *Journal of Ar-
870 chaeological Science* 38 (12), 3652–3661.
- 871 Benito-Calvo, A., Martínez-Moreno, J., Pardo, J. F. J., de la Torre, I., Torcal, R. M.,
872 2009. Sedimentological and archaeological fabrics in Palaeolithic levels of the
873 South-Eastern Pyrenees: Cova Gran and Roca dels Bous Sites (Lleida, Spain). *Jour-*
874 *nal of Archaeological Science* 36 (11), 2566 – 2577.
- 875 Benn, D., 1994. Fabric shape and the interpretation of sedimentary fabric data. *Journal*
876 *of Sedimentary Research* 64 (4a), 910–915.

- 877 Benvenuti, M., Martini, I. P., 2002. Analysis of terrestrial hyperconcentrated flows and
878 their deposit. In: Martini, I. P., Baker, V. R., Garzón, G. (Eds.), Flood and Megaflood
879 Processes and Deposits. Vol. 32 of Special Publication of the International Associa-
880 tion of Sedimentologists. Blackwell Publishing Ltd., pp. 167–193.
- 881 Berman, M., 1986. Testing for spatial association between a point process and another
882 stochastic process. *Applied Statistics* 35, 54–62.
- 883 Bernatchez, J. A., 2010. Taphonomic implications of orientation of plotted finds from
884 Pinnacle Point 13B (Mossel Bay, Western Cape Province, South Africa). *Journal of*
885 *Human Evolution* 59 (3–4), 274 – 288.
- 886 Bertran, P., Hetù, B., Texier, J.-P., Steijn, H. V., 1997. Fabric characteristics of subaerial
887 slope deposits. *Sedimentology* 44 (1), 1 – 16.
- 888 Bertran, P., Texier, J.-P., 1995. Fabric Analysis: Application to Paleolithic Sites. *Jour-*
889 *nal of Archaeological Science* 22 (4), 521 – 535.
- 890 Bevan, A., Crema, E., Li, X., Palmisano, A., 2013. Intensities, Interactions, and Un-
891 certainties: Some New Approaches to Archaeological Distributions. In: Bevan, A.,
892 Lake, M. (Eds.), Computational Approaches to Archaeological Spaces. Left Coast
893 Press, Walnut Creek, pp. 27–52.
- 894 Binford, L. R., 1981. Behavioral archaeology and the "pompeii premise". *Journal of*
895 *Anthropological Research* 37 (3), 195–208.
- 896 Boschian, G., Saccà, D., 2010. Ambiguities in human and elephant interactions? Sto-
897 ries of bones, sand and water from Castel di Guido (Italy). *Quaternary International*
898 214 (1–2), 3 – 16.
- 899 Brantingham, P. J., Surovell, T. A., Waguespack, N. M., 2007. Modeling post-
900 depositional mixing of archaeological deposits. *Journal of Anthropological Archae-
901 ology* 26 (4), 517 – 540.
- 902 Carrer, F., 2015. Interpreting Intra-site Spatial Patterns in Seasonal Contexts: an Eth-
903 noarchaeological Case Study from the Western Alps. *Journal of Archaeological*
904 *Method and Theory*, 1–25.
- 905 Cobo-Sánchez, L., Aramendi, J., Domínguez-Rodrigo, M., 2014. Orientation patterns
906 of wildebeest bones on the lake Masek floodplain (Serengeti, Tanzania) and their
907 relevance to interpret anisotropy in the Olduvai lacustrine floodplain. *Quaternary*
908 *International* 322–323 (0), 277 – 284.
- 909 de la Torre, I., Benito-Calvo, A., 2013. Application of GIS methods to retrieve ori-
910 entation patterns from imagery; a case study from Beds I and II, Olduvai Gorge
911 (Tanzania). *Journal of Archaeological Science* 40 (5), 2446–2457.
- 912 Dibble, H. L., Chase, P. G., McPherron, S. P., Tuffreau, A., Oct. 1997. Testing the
913 reality of a "living floor" with archaeological data. *American Antiquity* 62 (4), 629–
914 651.

- 915 Diggle, P., 1985. A kernel method for smoothing point process data. *Applied Statistics*
916 (Journal of the Royal Statistical Society, Series C) 34, 138–147.
- 917 Domínguez-Rodrigo, M., Bunn, H., Mabulla, A., Baquedano, E., Uribelarrea, D.,
918 Pérez-González, A., Gidna, A., Yravedra, J., Diez-Martín, F., Egeland, C., Barba,
919 R., Arriaza, M., Organista, E., Ansón, M., 2014a. On meat eating and human evolution:
920 A taphonomic analysis of BK4b (Upper Bed II, Olduvai Gorge, Tanzania), and
921 its bearing on hominin megafaunal consumption. *Quaternary International* 322–323,
922 129–152.
- 923 Domínguez-Rodrigo, M., Bunn, H., Pickering, T., Mabulla, A., Musiba, C., Baquedano,
924 E., Ashley, G., Diez-Martín, F., Santonja, M., Uribelarrea, D., Barba, R.,
925 Yravedra, J., Barboni, D., Arriaza, C., Gidna, A., 2012. Autochthony and orientation
926 patterns in Olduvai Bed I: a re-examination of the status of post-depositional biasing
927 of archaeological assemblages from FLK North (FLKN). *Journal of Archaeological
928 Science* 39 (7), 2116 – 2127.
- 929 Domínguez-Rodrigo, M., Cobo-Sánchez, L., Yravedra, J., Uribelarrea, D., Arriaza, C.,
930 Organista, E., Baquedano, E., 2017. Fluvial spatial taphonomy: a new method for the
931 study of post-depositional processes. *Archaeological and Anthropological Sciences*,
932 1–21.
- 933 Domínguez-Rodrigo, M., Diez-Martín, F., Yravedra, J., Barba, R., Mabulla, A., Baquedano,
934 E., Uribelarrea, D., Sánchez, P., Eren, M. I., 2014b. Study of the SHK Main
935 Site faunal assemblage, Olduvai Gorge, Tanzania: Implications for Bed II taphonomy,
936 paleoecology, and hominin utilization of megafauna. *Quaternary International*
937 322–323, 153–166.
- 938 Domínguez-Rodrigo, M., García-Pérez, A., 07 2013. Testing the Accuracy of Different
939 A-Axis Types for Measuring the Orientation of Bones in the Archaeological and
940 Paleontological Record. *PLoS ONE* 8 (7), e68955.
- 941 Domínguez-Rodrigo, M., Uribelarrea, D., Santonja, M., Bunn, H., García-Pérez, A.,
942 Pérez-González, A., Panera, J., Rubio-Jara, S., Mabulla, A., Baquedano, E., Yrave-
943 dra, J., Diez-Martín, F., 2014c. Autochthonous anisotropy of archaeological mate-
944 rials by the action of water: experimental and archaeological reassessment of the
945 orientation patterns at the Olduvai sites . *Journal of Archaeological Science* 41 (0),
946 44 – 68.
- 947 Eberth, D. A., Rogers, R. R., Fiorillo, A. R., 2007. A practical approach to the study of
948 bonebeds. In: Rogers, R. R., Eberth, D. A., Fiorillo, A. R. (Eds.), *Bonebeds. Genesis,*
949 *Analysis, and Paleobiological Significance*. The University of Chicago Press, pp.
950 265–332.
- 951 Enloe, J. G., 2006. Geological processes and site structure: assessing integrity at a late
952 paleolithic open-air site in northern france. *Geoarchaeology* 21 (6), 523–540.
- 953 Eren, M. I., Durant, A., Neudorf, C., Haslam, M., Shipton, C., Bora, J., Korisettar,
954 R., Petraglia, M., 2010. Experimental examination of animal trampling effects on

- 955 artifact movement in dry and water saturated substrates: a test case from South India.
956 Journal of Archaeological Science 37 (12), 3010 – 3021.
- 957 Fernández-López, S. R., 1991. Taphonomic concepts for a theoretical biochronology.
958 Revista Española de Paleontología 6, 37–49.
- 959 Fiorillo, A. R., 1991. Taphonomy and depositional setting of careless creek quarry (ju-
960 dith river formation), wheatland county, montana, u.s.a. Palaeogeography, Palaeo-
961 climatology, Palaeoecology 81 (3), 281–311.
- 962 García-Moreno, A., Smith, G. M., Kindler, L., Pop, E., Roebroeks, W., Gaudzinski-
963 Windheuser, S., Klinkenberg, V., 2016. Evaluating the incidence of hydrological
964 processes during site formation through orientation analysis. A case study of the
965 middle Palaeolithic Lakeland site of Neumark-Nord 2 (Germany). Journal of Ar-
966 chaeological Science: Reports 6, 82 – 93.
- 967 Giusti, D., Arzarello, M., 2016. The need for a taphonomic perspective in spatial analy-
968 sis: Formation processes at the Early Pleistocene site of Pirro Nord (P13), Apricena,
969 Italy. Journal of Archaeological Science: Reports 8, 235 – 249.
- 970 Harvati, K., Panagopoulou, E., Tourloukis, V., Thompson, N., Karkanas, P., Athanasi-
971 siou, A., Konidaris, G., Tsartsidou, G., Giusti, D., 2016. New Middle Pleistocene
972 elephant butchering site from Greece. In: Paleoanthropology Society Meeting. At-
973 lanta, Georgia, pp. A14–A15.
- 974 Hivernel, F., Hodder, I., 1984. Analysis of artifact distribution at Ngenym (Kenya):
975 depositional and postdepositional effects. In: Hietala, H., Larson, P. (Eds.), Intrasite
976 Spatial Analysis in Archaeology. Cambridge University Press, Ch. 7, pp. 97–115.
- 977 Hodder, I., Orton, C., 1976. Spatial Analysis in Archaeology. New Studies in Archae-
978 ology. Cambridge University Press, Cambridge.
- 979 Hovers, E., Ekshtain, R., Greenbaum, N., Malinsky-Buller, A., Nir, N., Yeshurun, R.,
980 2014. Islands in a stream? Reconstructing site formation processes in the late Middle
981 Paleolithic site of 'Ein Qashish, northern Israel. Quaternary International 331, 216–
982 233.
- 983 Isaac, G. L., 1967. Towards the interpretation of occupation debris: Some experiments
984 and observations. Kroeber Anthropological Society Papers 37 (37), 31–57.
- 985 Jammalamadaka, S., Sengupta, A., Sengupta, A., 2001. Topics in Circular Statistics.
986 Series on multivariate analysis. World Scientific.
- 987 Karkanas, P., Tourloukis, V., Thompson, N., Giusti, D., Panagopoulou, E., Harvati, K.,
988 this issue. Sedimentology and micromorphology of the lower palaeolithic lakeshore
989 site marathousa 1, megalopolis basin, greece. Quaternary International.
- 990 Kluskens, S. L., 1990. Orientation and density analysis of stone artefacts at combe-
991 capelle bas, périgord, france. Master's thesis, University of Pennsylvania.

- 992 Konidaris, G., Athanassiou, A., Tourloukis, V., Thompson, N., Giusti, D.,
993 Panagopoulou, E., Harvati, K., this issue. The skeleton of a straight-tusked elephant
994 (*Palaeoloxodon antiquus*) and other large mammals from the middle pleistocene lo-
995 cality marathousa 1 (megalopolis basin, greece): preliminary results. Quaternary
996 International.
- 997 Krumbein, W. C., 1941. Measurement and geological significance of shape and
998 roundness of sedimentary particles. JOURNAL OF SEDIMENTARY PETROLOGY
999 11 (2), 64–72.
- 1000 Lenoble, A., Bertran, P., 2004. Fabric of Palaeolithic levels: methods and implications
1001 for site formation processes. Journal of Archaeological Science 31 (4), 457 – 469.
- 1002 Lenoble, A., Bertran, P., Lacrampe, F., 2008. Solifluction-induced modifications
1003 of archaeological levels: simulation based on experimental data from a modern
1004 periglacial slope and application to French Palaeolithic sites. Journal of Archaeo-
1005 logical Science 35 (1), 99 – 110.
- 1006 Lindsay, J. F., 1968. The development of clast fabric in mudflows. Journal of Sedimen-
1007 tary Research 38 (4), 1242–1253.
- 1008 Macdonald, D. I. M., Jefferson, T. H., 1985. Orientation studies of waterlogged wood;
1009 a paleocurrent indicator? Journal of Sedimentary Research 55 (2), 235–239.
- 1010 Malinsky-Buller, A., Hovers, E., Marder, O., 2011. Making time: ‘Living floors’,
1011 ‘palimpsests’ and site formation processes – A perspective from the open-air Lower
1012 Paleolithic site of Revadim Quarry, Israel. Journal of Anthropological Archaeology
1013 30 (2), 89 – 101.
- 1014 Marwick, B., 2017. Computational reproducibility in archaeological research: Ba-
1015 sic principles and a case study of their implementation. Journal of Archaeological
1016 Method and Theory 24 (2), 424–450.
- 1017 Marwick, B., d’Alpoim Guedes, J., Barton, C. M., Bates, L. A., Baxter, M., Beavan,
1018 A., Bollwerk, E. A., Bocinsky, R. K., Brughams, T., Carter, A. K., Conrad, C.,
1019 Contreras, D. A., Costa, S., Crema, E. R., Daggett, A., Davies, B., Drake, B. L.,
1020 Dye, T. S., France, P., Fullager, R., Giusti, D., Graham, S., Harris, M. D., Hawks, J.,
1021 Heath, S., Huffer, D., Kansa, E. C., Kansa, S. W., Madsen, M. E., Melcher, J., Negre,
1022 J., Neiman, F. D., Opitz, R., Orton, D. C., Przystupa, P., Raviele, M., Riel-Salvatore,
1023 J., Riris, P., Romanowska, I., Smith, J., Strupler, N., Ullah, I. I., Vlack, H. G. V.,
1024 VanValkenberg, N., Watrall, E. C., Webster, C., Wells, J., Winters, J., Wren, C. D.,
1025 2017. Open science in archaeology. SAA Archaeological Record 17 (4), 8–14.
- 1026 McPherron, S. J., 2005. Artifact orientations and site formation processes from total
1027 station proveniences. Journal of Archaeological Science 32 (7), 1003 – 1014.
- 1028 McPherron, S. J., Dibble, H. L., Goldberg, P., 2005. Z. Geoarchaeology 20 (3), 243–
1029 262.

- 1030 Morton, A. G. T., 2004. Archaeological Site Formation: Understanding Lake Margin
1031 Contexts. No. 1211 in BAR International Series. Archaeopress, Oxford.
- 1032 Nickel, B., Riegel, W., Schonherr, T., Velitzelos, E., 1996. Environments of coal forma-
1033 tion in the Pleistocene lignite at Megalopolis, Peloponnesus (Greece) - reconstruc-
1034 tion from palynological and petrological investigations. N. Jb. Geol. Palaont. A. 200,
1035 201–220.
- 1036 Ohser, J., 1983. On estimators for the reduced second moment measure of point pro-
1037 cesses. Mathematische Operationsforschung und Statistik, series Statistics 14, 63–
1038 71.
- 1039 Organista, E., Domínguez-Rodrigo, M., Yravedra, J., Uribe Larrea, D., Arriaza, M. C.,
1040 Ortega, M. C., Mabulla, A., Gidna, A., Baquedano, E., 2017. Biotic and abiotic pro-
1041 cesses affecting the formation of BK Level 4c (Bed II, Olduvai Gorge) and their bear-
1042 ing on hominin behavior at the site. Palaeogeography, Palaeoclimatology, Palaeo-
1043 ecology, –.
- 1044 Orton, C., 1982. Stochastic process and archaeological mechanism in spatial analysis.
1045 Journal of Archaeological Science 9 (1), 1 – 23.
- 1046 Panagopoulou, E., Tourloukis, V., Thompson, N., Athanassiou, A., Tsartsidou, G.,
1047 Konidaris, G., Giusti, D., Karkanas, P., Harvati, K., 2015. Marathousa 1: a new Mid-
1048 dle Pleistocene archaeological site from Greece. Antiquity Project Gallery 89 (343).
- 1049 Petraglia, M. D., Nash, D. T., 1987. The impact of fluvial processes on experimen-
1050 tal sites. In: Nash, D. T., Petraglia, M. D. (Eds.), Natural formation processes and
1051 the archaeological record. Vol. 352 of International Series. British Archaeological
1052 Reports, Oxford, pp. 108–130.
- 1053 Petraglia, M. D., Potts, R., 1994. Water Flow and the Formation of Early Pleistocene
1054 Artifact Sites in Olduvai Gorge, Tanzania . Journal of Anthropological Archaeology
1055 13 (3), 228 – 254.
- 1056 Pierson, T. C., 2005. Distinguishing between debris flows and floods from field evi-
1057 dence in small watersheds. Usgs numbered series, U.S. Geological Survey.
- 1058 R Core Team, 2017. R: A Language and Environment for Statistical Computing. R
1059 Foundation for Statistical Computing, Vienna, Austria.
1060 URL <https://www.R-project.org/>
- 1061 Ripley, B., 1977. Modelling spatial patterns. Journal of the Royal Statistical Society,
1062 series B 39, 172–212.
- 1063 Ripley, B., 1988. Statistical inference for spatial processes. Cambridge University
1064 Press.
- 1065 Ripley, B. D., 1976. The second-order analysis of stationary point processes. Journal
1066 of Applied Probability 13 (2), 255–266.

- 1067 Ripley, B. D., 1981. Spatial Statistics. John Wiley and Sons, New York.
- 1068 Schick, K. D., 1984. Processes of paleolithic site formation: an experimental study.
1069 Ph.D. thesis, University of California, Berkeley.
- 1070 Schick, K. D., 1986. Stone Age sites in the making: experiments in the formation
1071 and transformation of archaeological occurrences. Vol. 319 of International Series.
1072 British Archaeological Reports, Oxford.
- 1073 Schick, K. D., 1987. Modeling the formation of Early Stone Age artifact concentra-
1074 tions. *Journal of Human Evolution* 16, 789–807.
- 1075 Schiffer, M. B., 1972. Archaeological Context and Systemic Context. *American Antiquity*
1076 37 (2), 156–165.
- 1077 Schiffer, M. B., 1983. Toward the identification of formation processes. *American Antiquity*
1078 48 (4), 675–706.
- 1079 Schiffer, M. B., 1987. Formation processes of the archaeological record. University of
1080 New Mexico Press, Albuquerque.
- 1081 Shackley, M. L., 1978. The behaviour of artefacts as sedimentary particles in a fluvial environment. *Archaeometry*
1082 20 (1), 55–61.
- 1083 Sánchez-Romero, L., Benito-Calvo, A., Pérez-González, A., Santonja, M., 12 2016.
1084 Assessment of Accumulation Processes at the Middle Pleistocene Site of Ambrona
1085 (Soria, Spain). Density and Orientation Patterns in Spatial Datasets Derived from
1086 Excavations Conducted from the 1960s to the Present. *PLOS ONE* 11 (12), 1–27.
- 1087 Texier, J.-P., 2000. A propos des processus de formation des sites préhistoriques / About
1088 prehistoric site formation processes. *Paléo* 12 (1), 379–386.
- 1089 Toots, H., 1965. Orientation and distribution of fossils as environmental indicators. In:
1090 Nineteenth Field Conference of the Wyoming Geological Association. pp. 219–292.
- 1091 Tourloukis, V., Thompson, N., Panagopoulou, E., Giusti, D., Konidaris, G., Karkanas,
1092 P., Harvati, K., this issue. Lithic and osseous artifacts from the lower palaeolithic site
1093 of marathousa 1, megalopolis, greece: preliminary results. *Quaternary International*.
- 1094 van Vugt, N., de Bruijn, H., van Kolfschoten, M., Langereis, C. G., 2000. Magneto-
1095 and cyclostratigraphy and mammal-fauna's of the Pleistocene lacustrine Megalopo-
1096 lis Basin, Peloponnesos, Greece. *Geologica Ultrajectina* 189, 69–92.
- 1097 Vaquero, M., Chacón, M. G., García-Antón, M. D., de Soler, B. G., Martínez, K.,
1098 Cuartero, F., 2012. Time and space in the formation of lithic assemblages: The
1099 example of Abric Romaní Level J. *Quaternary International* 247 (0), 162 – 181.
- 1100 Villa, P., 2004. Taphonomy and stratigraphy in european prehistory. *Before Farming*
1101 2004 (1), 1–20.

- 1102 Voorhies, M., 1969. Taphonomy and population dynamics of an early pliocene ver-
1103 tebrate fauna, knox county, nebraska. Contributions to Geology, University of
1104 Wyoming Special Paper 1, 1–69.
- 1105 Walter, M. J., Trauth, M. H., 2013. A {MATLAB} based orientation analysis of
1106 acheulean handaxe accumulations in olorgesailie and kariandusi, kenya rift. Jour-
1107 nal of Human Evolution 64 (6), 569 – 581.
- 1108 Wood, R. W., Johnson, D. L., 1978. A survey of disturbance processes in archaeologi-
1109 cal site formation. In: Schiffer, M. B. (Ed.), Advances in archaeological method and
1110 theory. Vol. 1. Academic Press, Ch. 9, pp. 315–381.
- 1111 Woodcock, N., Naylor, M., 1983. Randomness testing in three-dimensional orientation
1112 data. Journal of Structural Geology 5 (5), 539 – 548.